# Weak Tectono-Magmatic Relationships along an Obliquely Convergent Plate Boundary: Sumatra, Indonesia

Valerio Acocella, Olivier Bellier, Laura Sandri, Michel Sébrier, Subagyo Pramumijoyo

frontiers in Earth Science

ORIGINAL RESEARCH
published: 09 February 2018
doi: 10.3389/feart.2018.00003

# Weak Tectono-Magmatic Relationships along an Obliquely Convergent Plate Boundary: Sumatra, Indonesia

*Valerio Acocella*[1]*, *Olivier Bellier*[2], *Laura Sandri*[3], *Michel Sébrier*[4] and *Subagyo Pramumijoyo*[5]

[1] Dipartimento di Scienze, Università Roma Tre, Rome, Italy, [2] Aix Marseille Univ, CNRS, IRD, INRA, Coll France, CEREGE, Aix-en-Provence, France, [3] Istituto Nazionale Geofisica e Vulcanologia, Sezione Bologna, Italy, [4] Centre National de la Recherche Scientifique, Institut des Sciences de la Terre de Paris (ISTeP), UPMC Univ Paris 06, Sorbonne Universités, Paris, France, [5] Geological Engineering Department, Faculty of Engineering, Universitas Gadjah Mada, Yogyakarta, Indonesia

The tectono-magmatic relationships along obliquely convergent plate boundaries, where strain partitioning promotes strike-slip structures along the volcanic arc, are poorly known. Here it is unclear if and, in case, how the strike-slip structures control volcanic processes, distribution and size. To better define the possible tectono-magmatic relationships along strike-slip arcs, we merge available information on the case study of Sumatra (Indonesia) with field structural data. The Sumatra arc (entire volcanic belt) consists of 48 active volcanoes. Of these, 46% lie within 10 km from the dextral Great Sumatra Fault (GSF), which carries most horizontal displacement on the overriding plate, whereas 27% lie at >20 km from the GSF. Among the volcanoes at <10 km from GSF, 48% show a possible structural relation to the GSF, whereas only 28% show a clear structural relation, lying in pull-aparts or releasing bends; these localized areas of transtension (local extensional zone) do not develop magmatic segments. There is no relation between the GSF along-strike slip rate variations and the volcanic productivity. The preferred N30°-N40°E volcano alignment and elongation are subparallel to the convergence vector or to the GSF. The structural field data, collected in the central and southern GSF, show, in addition to the dextral motions along NW-SE to N-S striking faults, also normal motions (extending WNW-ESE or NE-SW), suggesting local reactivations of the GSF. Overall, the collected data suggest a limited tectonic control on arc volcanism. The tectonic control is mostly expressed by the mean depth of the slab surface below the volcanoes (130 ± 20 km) and, subordinately, local extension along the GSF. The latter, when WNW-ESE oriented (more common), may be associated with the overall tectonic convergence, as suggested by the structural data; conversely, when NE-SW oriented (less common), the extension may result from co- and post-seismic arc normal extension, as supported by the 2004 mega-earthquake measurements. Overall, the strike-slip arc of Sumatra has intermediate features between those of extensional and contractional arcs.

**Keywords: oblique convergence, strain partitioning, strike-slip faulting, volcanism, Sumatra**

OPEN ACCESS

***Edited by:***
*Alessandro Tibaldi, Università Degli Studi di Milano Bicocca, Italy*

***Reviewed by:***
*Luis E. Lara, Sernageomin, Chile*
*Federico P. Mariotto, University of Insubria, Italy*

***Correspondence:**
*Valerio Acocella*
*acocella@uniroma3.it*

***Specialty section:***
*This article was submitted to Structural Geology and Tectonics, a section of the journal Frontiers in Earth Science*

***Received:*** *02 November 2017*
***Accepted:*** *15 January 2018*
***Published:*** *09 February 2018*

***Citation:***
*Acocella V, Bellier O, Sandri L, Sébrier M and Pramumijoyo S (2018) Weak Tectono-Magmatic Relationships along an Obliquely Convergent Plate Boundary: Sumatra, Indonesia. Front. Earth Sci. 6:3. doi: 10.3389/feart.2018.00003*

## INTRODUCTION

The relations between magmatism and regional tectonics have been object of several studies in the last decades, especially along divergent plate boundaries, where the crucial role of magmatism on the development of the plate boundary has been repeatedly highlighted. In fact, recent diking episodes in Afar (Asal-Ghoubbet, 1978; Dallol, 2004; Dabbahu, 2005), Iceland (Krafla, 1975-1984; Bárðarbunga, 2014), Tanzania (Lake Natron, 2007) and Red Sea (Harrat Lunayyr, 2009; southern Red Sea, 2011-2013) have shown the importance of transient magmatic events in the opening of rift zones (e.g., Ruegg et al., 1979; Rubin and Pollard, 1988; Tryggvason, 1994; Wright et al., 2006; Calais et al., 2008; Pallister et al., 2010; Nobile et al., 2012; Sigmundsson et al., 2015; Xu et al., 2015). These intrusions cluster in magmatic segments parallel to the rift axis, which are characterized by the focusing of tectonic and magmatic activity, with the development of rift-parallel eruptive fissures (Gudmundsson, 1995; Ebinger and Casey, 2001; Acocella, 2014).

Our knowledge on the tectono-magmatic relationships in volcanic arcs along convergent plate boundaries is less advanced, and depends on the kinematics of the structures along the arc, which usually reflects the overall plate motion convergence (Acocella and Funiciello, 2010). Magma-assisted processes similar to those observed in rifts may occur also along magmatic arcs experiencing extension, as the Taupo Volcanic Zone of New Zealand (Acocella et al., 2003; Rowland et al., 2010; Allan et al., 2012). Indeed, the tectono-magmatic architecture of "highly" extending arcs (∼1 cm/year or more) is similar to that of moderately extending continental rifts (Acocella, 2014). Contractional arcs are less common: along the contractional arc of NE Japan proper arc-parallel magmatic systems are lacking and the linear mode of magmatic accretion below the arc becomes generally punctiform at the surface (Acocella et al., 2008; Acocella, 2014). Many magmatic arcs are also characterized by significant strike-slip motion promoted by strain partitioning induced by the oblique convergence between the two interacting plates (e.g., McCaffrey, 1992; Lallemant, 1996; Acocella and Funiciello, 2010): examples include the Southern Andes, the Central American Volcanic Arc, the Mexican Trans Volcanic Belt, the Philippines, the Kurile arc and the Sumatra arc. These arcs undergoing strike-slip motions are known only in their very general features, with volcanism inferred to be often associated with local extension created by the activity of pull-aparts, releasing bends or dilational jogs (i.e., DeMets, 1992; Tibaldi, 1992; Ego and Ansan, 2002; Pasquarè and Tibaldi, 2003; Corti et al., 2005; Rosenau et al., 2006; Cembrano and Lara, 2009; Tibaldi et al., 2010; Shabanian et al., 2012). These general relations between volcanism and strike-slip structures are largely confirmed by the deeper structure of extinct and eroded magmatic arcs: there pluton emplacement has been most commonly associated with the local extension created by strike-slip systems (e.g., Tobisch and Cruden, 1995; Acocella and Funiciello, 2010, and references therein). However, recent studies on active volcanic arcs inferred to experience significant strike-slip motion, as the central Aeolian arc (Italy; De Astis et al., 2003), suggest a tectonic reorganization with predominant magma-induced extension at the surface, without evident strike-slip faulting (Ruch et al., 2016).

The Sumatra arc shows a significant obliquity and, as such, it constitutes an ideal site to understand and define the tectono-magmatic relationships in strike-slip arcs. Here the available information suggests that volcanism focuses along major strike-slip systems (Bellier and Sébrier, 1994; Bellier et al., 1999): however, detailed studies are lacking, so that the exact relationships between strike-slip structures and magmatism remain elusive, leaving a crucial knowledge gap (Acocella, 2014, and references therein). Indeed, despite the general spatial coincidence between the location of strike-slip faulting (along the dextral Great Sumatra Fault, or GSF) and volcanic activity, there are very limited data describing the local structural control on volcanism: knowledge gaps include the definition of the existence, configuration, shape and size of the magmatic systems, the definition of the relationships between the main tectonic structures and the rise, emplacement and eruption of magma. Also, the presence of large magmatic systems, as below the huge Toba caldera, lying a few tens of km to the east of the GSF (see section below; Genrich et al., 2000) constitutes a puzzling context to explain any structural control on volcanic activity. Therefore, more studies are needed to evaluate the detailed relationships between the development of GSF and the volcanoes on Sumatra.

These important gaps should be filled also to define the tectono-magmatic relationships of arcs in strike-slip settings and place these in the broader context considering the different kinematics of the plate boundaries and, in turn, relate these to their magmatic outcome, providing a comprehensive framework (e.g., Chaussard and Amelung, 2012). The latter should also take into account for the possibility of transient kinematic inversions during and after mega-earthquakes, as observed in NE Japan after the 2011 Tohoku earthquake (Ozawa et al., 2011; Simons et al., 2011; Takada and Fukushima, 2013) and in Southern Chile (Sepulveda et al., 2005; Vigny et al., 2011; Pritchard et al., 2013; Lupi and Miller, 2014). In both cases, mega-earthquakes promoted the transient (co- and post-seismic) inversion of the major tectonic structures, also affecting magmatic activity (Lara et al., 2004; Takada and Fukushima, 2013). In fact, earthquake-induced extension along volcanic arcs may enhance diking, bubble nucleation, magma mixing and thus increase the possibility of an eruption (Walter and Amelung, 2007). Understanding how these transient kinematic variations may affect the structure of a volcanic arc is also crucial to explain the presence and orientation of apparently anomalous volcanic features, otherwise not easily reconciled with the longer-term inter-seismic kinematics of an arc.

This study aims at: (1) better defining the main structural (including distribution, geometry and kinematics of the main structures) and volcanic (including volcano type, elongation, distribution, alignment, volume) features of the volcanic arc of Sumatra and (2) to consider their possible relationships, in order to propose a general tectono-magmatic model of Sumatra. To this aim, we use available tectonic, structural and volcanological data, matched with original structural data collected at two selected portions of the volcanic arc. The obtained results are briefly considered in a more general framework relating the

tectono-magmatic model proposed for Sumatra to that available for extensional and contractional arcs, as well as for divergent plate boundaries.

## TECTONIC SETTING OF SUMATRA

Sumatra exposes part of the oblique convergent boundary between the Indian and Eurasian plates; while contraction dominates on the offshore portion, the Great Sumatra Fault (GSF) carries most of the onland strain, with predominant dextral motion; this highlights an almost full partitioning of the deformation (dip-slip motion in the proximal part of the overriding plate, toward the trench, and strike-slip motion in the distal portion of the plate, along the magmatic arc; **Figure 1**; e.g., Bellier and Sebrier, 1995; Baroux et al., 1998; Bellier et al., 1999; McCaffrey et al., 2000; Bradley et al., 2017). The GSF propagated southwards, in central-southern Sumatra, from ∼2 Ma (**Figure 1**; Sieh and Natawidjaja, 2000). It is usually active as a vertical plane down to depths of ∼15 km, as revealed by the associated seismicity arriving nearly to the base of the considerably brittle crust (e.g., Widiwijayanti et al., 1996; Genrich et al., 2000; Natawidjaja and Triyoso, 2007; Weller et al., 2012). No information is available on the continuation of the GSF within the ductile crust, even though recent studies in similar tectonic settings (South Chile subduction zone) suggest a curving of the fault at depth (Catalan et al., 2017). The GSF is segmented and consists of at least 19 major NW-SE trending subparallel branches, also forming strike-slip duplexes, with a northward increase of segment length and slip rate from 5 to 26 mm/year (**Figure 1**; Bellier et al., 1991, 1997; Duquesnoy et al., 1996; Genrich et al., 2000; Prawirodirdjo et al., 2000; Sieh and Natawidjaja, 2000; Natawidjaja and Triyoso, 2007; Nakano et al., 2010; Weller et al., 2012; Ito et al., 2016; Bradley et al., 2017). Overall, most (>80%) of the GSF consists of a narrow (a very few km wide) zone of deformation along a main dextral segment; limited parts (<20%) of the GSF may show offset segments, overlapping at times, or may be only inferred (Sieh and Natawidjaja, 2000, and references therein). Geomorphic offsets along the fault range as high as 20 km and may represent only the most recent displacement, with other unidentified structures having accommodated the dextral component of oblique convergence in the last million years (Sieh and Natawidjaja, 2000). Interaction between offset dextral segments along the GSF creates repeated areas of localized extension (e.g., Nakano et al., 2010), in a context of overall NNE-SSW trending maximum compression (Mount and Suppe, 1992). Outside the GSF (at its southern termination), the main extensional structures on Sumatra, NNE-SSW to NE-SW oriented, are subparallel to this maximum compression (Pramumijoyo and Sébrier, 1991).

Arc volcanism has been accompanying convergence at least from the Mesozoic. While the Late Miocene volcanism in northern Sumatra is scattered, in the southern part volcanism focuses to the west, generally overlapping with the Quaternary volcanism, even though the latter is possibly more shifted to the west (Rock et al., 1982). An important part of the Quaternary volcanism focuses along the GSF (**Figure 1**; Sieh and Natawidjaja, 2000). Quaternary volcanics are mainly calc-alkaline andesites, dacites, and rhyolites with few basalts; their overall composition is genetically homogeneous, derived from <10% of assimilation of crustal material by uprising melts from the Indian Ocean-type mantle wedge (Rock et al., 1982; Gasparon and Varne, 1998; Gasparon, 2005). The mean spacing between volcanoes shows two peaks at ∼25 km and ∼65 km (de Bremond d'Ars et al., 1995). Most volcanoes consist of stratovolcanoes or composite volcanic edifices, with monogenic vents on their flanks. At times, calderas are also present. The magmatic arc may locally help the partitioning process by localizing the margin-parallel shear strain in the upper plate, controlling the rupture process and seismic moment release along the GSF (Widiwijayanti et al., 1996; McCaffrey et al., 2000).

The overall relationships between the Sumatran volcanic arc and the GSF are unclear. On the one hand, the volcanic arc focuses in correspondence to the GSF, which may influence the distribution of the volcanoes (e.g., Bellier and Sébrier, 1994). On the other hand, some studies suggest that the Sumatra fault zone and the volcanic arc act independently and that the proximity of the volcanoes to the fault is a "random occurrence" (Sieh and Natawidjaja, 2000): for example, out of 50 active volcanoes, only 9 are within 2 km of the GSF, while the rest lie at an average of 10 km from the fault at the surface. Accordingly, the distribution of volcanoes relative to the GSF suggests that the modern magmatic arc should have not created any weak crustal zone that has favored the concentration of shear (Sieh and Natawidjaja, 2000). Also, immediately north of Sumatra, in the Banda Aceh region, the volcanic arc is shifted eastward (in the extensional Weh Basin) with regard to the northern continuation of the GSF, partitioned in a western contractional zone and an eastern dextral zone (Ghosal et al., 2012; Fernandez-Blanco et al., 2016). Even though the latter may postdate the volcanic arc, here there is no evidence of a direct link between the GSF and volcanism.

The largest and most representative volcanic complex is Toba Caldera, located along a major bend in the subducting plate below, probably characterized by a tear reactivating a pre-existing fracture zone (**Figure 1**; Fauzi et al., 1996; Pesicek et al., 2008; Hall and Spakman, 2015; Koulakov et al., 2016). Toba is the site of Earth's largest Quaternary eruption, ejecting ∼3000 $km^3$ of magma, after at least 150,000 years of storage and evolution (Vazquez and Reid, 2004; De Silva et al., 2015). The caldera has an elliptical shape with a pronounced NW-SE elongation, parallel to the nearby GSF segment, and it has been interpreted as due to a presently inactive stepover between dextral segments (Detourbet et al., 1993). However, the structural relationships between the GSF segment and the caldera structure are not obvious; in fact, the segment lies ∼10 km to the SW of the western caldera rim, and geodetic modeling shows that slip of the GSF segment currently focuses several km SW of the geologic fault plane (Genrich et al., 2000). The magma reservoir below the caldera consists of stacked sills down to a depth of 7 km; this reservoir lies on top of a low velocity anomaly almost extending down to the top of the slab (Sakaguchi et al., 2006; Koulakov et al., 2009; Stankiewicz et al., 2010; Chesner, 2012, and references therein;

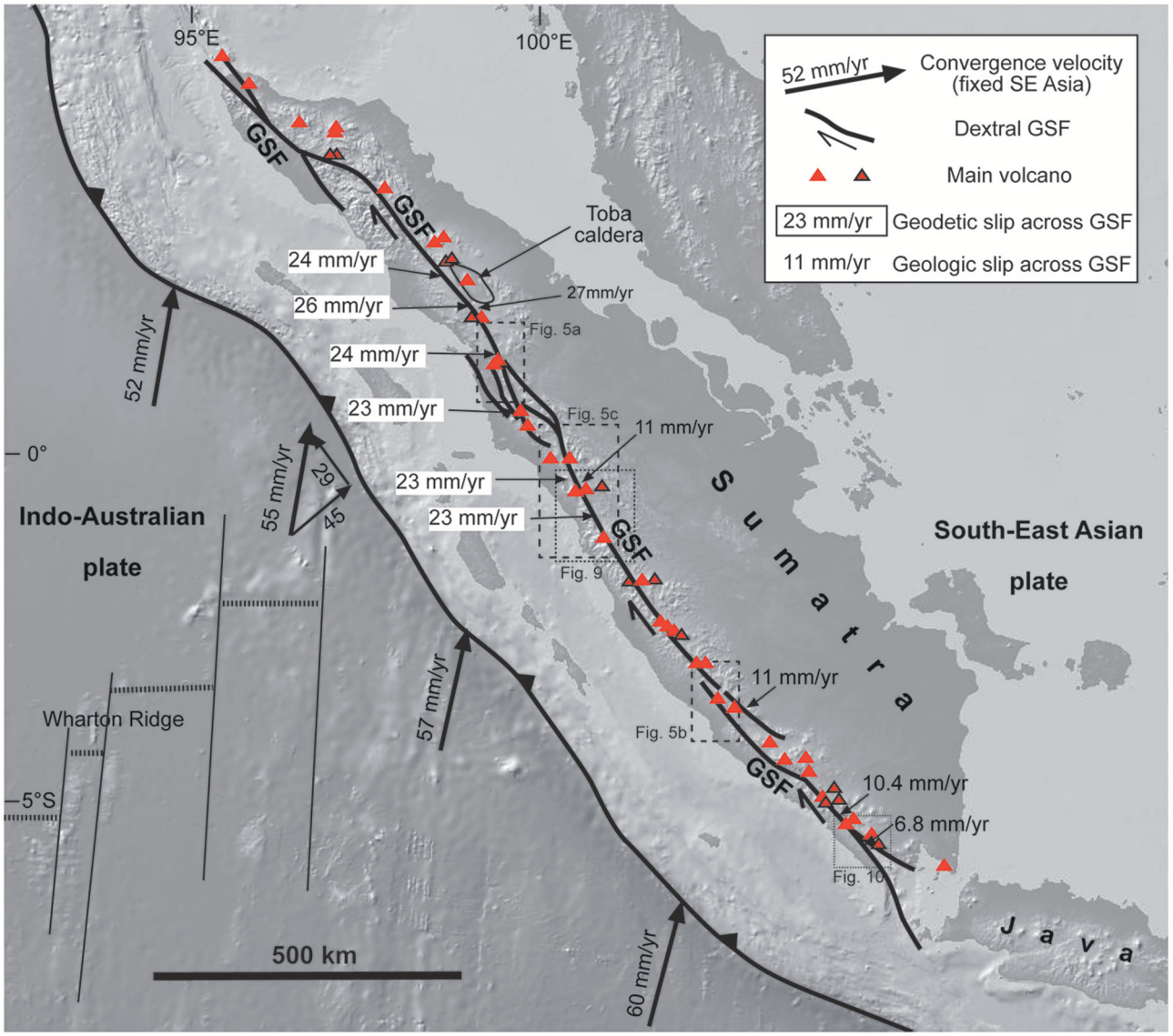


**FIGURE 1 |** Overview of Sumatra Island, showing the location of the active volcanoes (red triangles from the Smithsonian Global Volcanism Program, red triangles with black frame from Sieh and Natawidjaja, 2000) considered in this study and the GSF.

Jaxybulatov et al., 2014). Other volcanic areas host calderas (as Ranau caldera; Bellier and Sébrier, 1994; Natawidjaja et al., 2017), stratovolcanoes (between 600 and 3800 m high), domes and geothermal activity (Gasparon, 2005). The latter includes the Sarulla graben (Hickman et al., 2004) and the Tarutung and Silangkitang geothermal areas, where the fluid pathways are related to pull-aparts (Muksin et al., 2013, 2014), negative flowers (Nukman and Moeck, 2013) and subvertical (Moore et al., 2001) splays of the GSF. In the latter case, the geothermal reservoir appears centered along the fault zone, where the highly fractured and hydrothermally altered rocks serve as main conduits for vertical fluid flow from deeper magmatic sources (Moore et al., 2001). The geothermal and other volcanic areas seem mostly located along splays of the GSF, inferred to carry local extension in between, possibly above active shallow magma chambers, at 1–3 km depth (Widiwijayanti et al., 1996; Bellier et al., 1999; Chaussard and Amelung, 2012).

The most recent evolution of Sumatra has been characterized by widespread seismicity, with seismic hazard being expected to increase northwards (Beaudoin et al., 1995; Bellier et al., 1997). A narrow seismic gap characterized the volcanic areas during the aftershock sequence of the 1994 M6.8 Liwa earthquake, in southern Sumatra, suggesting that the rupture process is also controlled by the location of magma (Widiwijayanti et al., 1996).

GPS data in the northern part of Sumatra show that the co- and post-seismic displacement after the 2004 M9.2 Sumatra-Andaman mega-earthquake was characterized by significant SW motion (several tens of cm of co-seismic displacement, plus tens

of cm in the first year after the earthquake) of the volcanic arc region (Subarya et al., 2006; Gahalaut et al., 2008; Shearer and Burgmann, 2010). The 2004 mega-earthquake was followed, 1 month later, by a seismic swarm in the Andaman Sea north of Sumatra (Kundu et al., 2012) and volcanism, as testified by a submarine eruption (Kamesh Raju et al., 2012). In particular, this seismicity is at first consistent with the regional tectonic setting and, subsequently, with the involvement of fluids, also magmatic, producing normal faults along a NNE-SSW direction (Kundu et al., 2012).

Limited information is available on the depth to the magma reservoirs below the volcanoes of Sumatra. The inversion of InSAR data from two Sumatran volcanoes inflating from 2006 to 2009 suggests very shallow magmatic sources, at depth of 1 km or less (Chaussard and Amelung, 2012).

## METHODOLOGY

Here we review and discuss the available data concerning the tectono-magmatic features of western Sumatra, in particular those regarding the tectonic setting of the plates (obliquity variations in convergence, depth of the slab surface below the volcanic arc, trench distance from the volcanic arc and the GSF), the structure of the GSF (slip rate, fault configuration) and the volcanic arc (distribution of active volcanoes, volcano elongation and vent alignment, minimum erupted volumes); these features have been mostly quantified and summarized in **Table 1**, which includes also an essential reference list.

The considered tectonic and structural data have been largely published (Bellier et al., 1999; Genrich et al., 2000; Sieh and Natawidjaja, 2000; Natawidjaja and Triyoso, 2007); these studies highlight the current static geometry of the GSF, neglecting any longer-term variation, due to the evolution of stepovers, pull-aparts and relay zones, as highlighted by Bellier and Sébrier (1994), or of the plate tectonic boundary variations (Detourbet, 1995).

The volcanic data have been extracted and quantified considering available digital elevation models (largely taken from GeoMapApp; http://www.geomapapp.org), satellite images available on Google Earth (https://www.google.com/earth/); geological maps from the Geological Research and Development Centre, Bandung (usually at the 1:100,000 scale, plus more detailed maps on selected volcanoes at the 1:25,000 and 1:50,000 scale). The selection of the Quaternary volcanoes has been made merging the data from the Smithsonian Global Volcanism Program (SGVP; http://volcano.si.edu) and the information contained in the detailed study of Sieh and Natawidjaja (2000); the latter includes 13 more volcanoes with respect to the SGVP database, inferred to be <100,000 years old. Both the elongation of the volcanic edifice and the alignment of the flank vents within have been used to try to define the preferred structural control of the volcano, in order to try to relate this to the known structural trends in Sumatra. The erupted volumes refer, in absence of more precise information, to the volume of the volcanic edifice, or of the depression hosting the caldera; these provide minimum estimates of the erupted volumes and should, with the exception of the volumes erupted at Toba, not be considered as Dense Rock Equivalent (non-DRE; see caption of **Table 1**). The uncertainties related to these volume estimates (due to erosion, burial, unknown thicknesses, ash dispersal) are common to all the volcanoes, providing a recurrent and systematic bias in our analysis. Therefore, as these minimum volume estimates are considered in a relative way, they can be used to compare the relative production along the volcanic arc. For details on the related errors, see **Table 1**.

In addition, we present original structural field data collected along the central and southern portions of the GSF (location shown by dotted boxes in **Figure 1**). The structural field data, seldom reported in the literature, allow better characterizing the deformation pattern of the GSF. The faults have been kinematically characterized, using slip data obtained from the identification and measurement of the slickenlines on the fault planes. Measurements involved the determination of the pitch and possible sense of motion. The latter was determined considering the presence and orientation of micro- and meso-indicators on the fault plane (e.g., Fossen, 2010). The slip data are derived from the pitch of the slickenlines, that is the angle which a fabric makes to the strike direction. Here we use the convention that pitch values range from $-90^\circ$ to $+90^\circ$; these correspond to pure strike-slip motions, whereas pitches $= 0^\circ$ correspond to pure dip-slip motions.

The structural data have been also inverted to infer the possible stress field. To determine states of stress, we performed a quantitative inversion of distinct families of fault slip data measured at each individual site, using the method originally proposed by Carey (1979). This fault kinematics inversion method computes a mean best fitting deviatoric stress tensor from a set of striated faults by minimizing the angular deviation (misfit angle) between a predicted slip-vector and the observed striation (Carey, 1979). The inversion results include the orientation (azimuth and plunge) of the principal stress axes ($\sigma_1 > \sigma_2 > \sigma_3$, corresponding to maximum, intermediate and minimum stress axis, respectively) (e.g., Carey and Brunier, 1974; Mercier et al., 1991; Bellier and Zoback, 1995, and references therein).

## RESULTS

### General Tectono-Magmatic Features of the arc

Available data highlight a vertical geometry of the GSF in the brittle crust (e.g., Weller et al., 2012), suggesting that the surface trace of the GSF is representative of its location in the upper crust. Moreover, the extremely focused (very few km wide) area of deformation along the GSF (Sieh and Natawidjaja, 2000) suggests that the distance of a volcano from the fault can help discriminating any structural control of the GSF on volcanism. Basing on these considerations, the distribution of the 48 Quaternary volcanoes with regard to the location of the GSF at the surface in Sumatra is considered and summarized in **Figure 2A**. This shows that, while 46% of the volcanoes lie at <10 km from the GSF, 27% lie at >20 km from the

**TABLE 1 |** Summary of the main tectonic, structural and magmatic features of the active volcanoes on Sumatra. See text for details.

| Active volcano (N to S) | Distance (km)/ Source | Slab depth (km, ±5) | Trench distance | GSF distance | GSF tectonic control | Elongation direction (°) | Vent alignment (°) | Erupted volume ($km^3$) | GSF slip (mm/year) |
|---|---|---|---|---|---|---|---|---|---|
| Seulawah Agam | 36; SGVP | 130 | 290 | 4 | | −86 | 31 | 21.3 | 13[d] |
| Peuet Sugue | 131; SGVP | 155 | 320 | 22 | | 30 | 37 | 76.9 | 38[c] |
| Geureudong | 186; SGVP | 185 | 330 | 50 | | 0 | 17 | 253.4* | 38[c] |
| Telong Bur Ni | 189; SGVP | 180 | 320 | 45 | | NA | 30 | | 38[c] |
| Takengon | 192; Sieh | 165 | 305 | 31 | | 31 | 36 | 30.1 | |
| Br Alur | 212; Sieh | 145 | 290 | 9 | | −70 | (18), −18, −73 | 68,1 | |
| Kembar | 318; SGVP | 130 | 290 | 12 | Possible link to GSF | 21 | 20 | 52.8 | 27[b] |
| Sinabung | 431; SGVP | 130 | 300 | 31 | | (14) | 33 | 16.7 | 27[b] |
| Singkut | 443; SGVP | 145 | 315 | 37 | | −52 | −50, 34 | 26.2 | 27[b] |
| Toba Nord | 462; Sieh | 130 | 305 | 34 | | −22 | (−8), −33 | 3.3 | 27[b] |
| Toba West | 495; Sieh | 105 | 280 | 12 | | −18 | NA | 23.3 | 27[b] |
| Toba caldera | 509; SGVP | 120 | 295 | 25 | | −42 | −40 (res. dom.) | >2,800; >5,600° | 27[b] |
| Imun | 547; SGVP | 115 | 285 | 4 | Possible link to GSF | 3 | NA | 2.3 | 24[b] |
| Martimbang | 564; Sieh | 105 | 280 | −2 | Probable link to GSF | (14) | 17 | 3.9 | 24[b] |
| Sibualbuali | 617; SGVP | 130 | 285 | 3 | Pull-apart-rel. bend | −14 | −5 | 56.4 | 23[b] |
| Lubukraya | 622; SGVP | 125 | 275 | −3 | Pull-apart-rel. bend | 55 | 0, 58 | 113.9 | 23[b] |
| Sorikmarapi | 715; SGVP | 135 | 280 | −3 | | −27 | −27 | 353.4 | 23[b] |
| Sorik-Malintang | 743; SGVP | 140 | 275 | −12 | | (39) | (39) | 157.1 | 23[b] |
| Talakmau | 794; SGVP | 140 | 275 | −19 | | 37 | 40 | 301.6 | 23[d] |
| Sarik Gajah | 826; SGVP | 145 | 295 | 1 | Pull-apart-rel. bend | NA | 41 | 0.2 | 11[b] 23[d] |
| Tandikat | 864; SGVP | 130 | 285 | −6 | | 21 | 21 | 113.9 | 12[c] 23[d] |
| Marapi | 872; SGVP | 140 | 295 | 7 | Possible link to GSF | 38 | 38 | 230.4 | 12[c] 23[d] |
| Malintang-Sago | 878; Sieh | 165 | 315 | 29 | | (32) | NA | 190.1 | 12[c] 23[d] |
| Talang | 941; SGVP | 130 | 280 | −1 | Pull-apart-rel. bend | −66 | −88, 33 | 49 | 11[b] 23[d] |
| Melenggok | 1020; Sieh | 130 | 255 | −2 | Pull-apart-rel. bend | −54 | −54 | 40 | 11[c] 23[d] |
| Kerinci | 1045; SGVP | 140 | 270 | 9 | | 45 | 30 | 240.8 | 11[c] 23[d] |
| Tujuh | 1049; Sieh | 150 | 285 | 22 | | −44 | −43 | 152 | 11[c] 23[d] |
| Kunyit | 1108; SGVP | 115 | 255 | −1 | Pull-apart-rel. bend | 21 | NA | 31.4 | 11[c] 23[d] |
| Hutapanjang | 1119; SGVP | 120 | 260 | 5 | Possible link to GSF | NA | NA | (4.7) | 11[c] |
| Sumbing | 1133; SGVP | 120 | 260 | 9 | | (26) | (33) | 20.1 | 11[c] |
| Kumbang | 1145; Sieh | 125 | 275 | 20 | | 62 | 64 | 253 | 11[c] |
| Pendan | 1189; SGVP | 120 | 255 | 2 | Possible link to GSF | NA | NA | NA | 11[c] |
| Belinrang | 1196; SGVP | 125 | 275 | 12 | | NA | NA | NA | 11[c] |
| Daun Bukit | 1262; SGVP | 110 | 255 | −1 | Probable link to GSF | NA | 67, 12 | 152, 7 | 11[b] |
| Kaba | 1290; SGVP | 125 | 275 | 1 | Possible link to GSF | 57 | 65 | 93.8 | 11[b] |
| Dempo | 1378; SGVP | 130 | 270 | 14 | | −61 | −64 | 219.9 | |
| Patah | 1411; SGVP | 120 | 280 | 2 | Possible link to GSF | NA | NA | NA | |
| Lumut Balai | 1426; SGVP | 145 | 300 | 14 | | 19 | (16) | 110.2 | |
| Besar | 1449; SGVP | 130 | 290 | 1 | Possible link to GSF | 34 | 30 | 105.6 | |
| Ranau | 1495; SGVP | 110 | 270 | 0 | Possible link to GSF | 36 | NA | (205) | 5.5[a] |
| Seminung | 1501; Sieh | 105 | 270 | −2 | Probable link to GSF | NA | 63 | 31.4 | 5.5[a] |
| Raja | 1507; Sieh | 120 | 285 | 12 | | 57 | NA | 37.7 | 5.5[a] |
| Pesagi | 1520; Sieh | 115 | 290 | 8 | | −8 | (0) | 45.2 | 5.5[a]-10.4[e] |
| Sekincau Belirang | 1546; SGVP | 110 | 270 | 9 | | (−17) | −24 | 46.1 | |
| Suoh | 1557; SGVP | 95 | 260 | 1 | Pull-apart-rel. bend | (10) | 10 | >7 | 6.8[e] |

*(Continued)*

**TABLE 1** | Continued

| Active volcano (N to S) | Distance (km)/ Source | Slab depth (km, ±5) | Trench distance | GSF distance | GSF tectonic control | Elongation direction (°) | Vent alignment (°) | Erupted volume ($km^3$) | GSF slip (mm/year) |
|---|---|---|---|---|---|---|---|---|---|
| Hulubelu | 1598; SGVP | 105 | 270 | 20 | | NA | (−23) | >2 | |
| Sekincau | 1609; Sieh | 105 | 275 | 22 | | −52 | −54 | 169.6 | |
| Rajabasa | 1705; SGVP | 175 | 280 | 94 | | −61 | NA | 101.8 | |

*Distance of volcano: distance from the NW tip of Sumatra (Banda Aceh town).*
*Source of volcano: SGVP = Smithsonian Global Volcanism Program, eruptions <10 ka; Sieh = Sieh and Natawidjaja (2000), <100 ka.*
*Slab depth from Sieh and Natawidjaja (2000).*
*Trench and GSF distances in km.*
*Trench distance = distance of volcano from nearest trench portion.*
*Distance from GSF = distance of volcano from the nearest active segment of GSF (positive values are to the east of the fault).*
*Elongation direction of edifice in degrees relative to N (negative values are westward); NA = circular edifice.*
*Vent alignment also includes direction of structures; when less constrained is in brackets; NA = no available data.*
*Erupted volumes of edifices (only proximal deposits, not distal) non DRE, except for Toba caldera (however, value for Toba ° = non DRE, assuming a correction of 0.5 (Rose and Chesner, 1987); error = 20% for stratovolcanoes; error for calderas and volcanoes in brackets may be as high as 50%.*
**= with Telong Bur Ni.*
*Slip rates in red are geological; rates in black are geodetic. References: [a]= Bellier et al., 1999; [b]= Sieh and Natawidjaja (2000); [c]= Genrich et al., 2000, and references therein; [d]= Natawidjaja and Triyoso, 2007; [e]= Natawidjaja et al., 2017.*

GSF; a similar distribution was already proposed by Sieh and Natawidjaja (2000). The histogram in the inset of **Figure 2A** shows how, excluding the volcanoes at distance <10 km from the GSF, with the exception of the three volcanoes with the highest negative distance, all the remaining volcanoes are located to the east of the GSF; this indicates that, despite the general SE decrease in the arc-trench gap, approximately one third of the volcanoes does not have any clear connection with the GSF. To investigate whether there is any correlation with the general tectonic setting, we report the location of the volcanoes as a function of the distance from the trench (**Figure 2B**) and the depth of the slab surface (**Figure 2C**). There is a slight southward decrease in the distance of the volcanoes from the trench, from 290 to 330 km at the northern tip of Sumatra to the 260–300 km at the southern tip (**Figure 2B**). This decrease may be related to the overall higher dip of the slab below the southern part of the island, as supported by tomographic data (Hall and Spakman, 2015). The average depth of the slab below the volcanoes seems to slightly decrease southward (**Figure 2C**), even though with a less evident gradient and higher scatter. The frequency distribution in the inset in **Figure 2C** shows an approximately normal distribution and suggests that the most common depth of the slab below the volcanoes is 130 ± 20 km, even though several outliers exist, especially to the east.

The slab depth is representative of the stability of the hydrated minerals, and thus of the release of the fluids generating the magmas at shallower levels; therefore, the depth of the slab below the volcanoes may control their location. This implies that the lateral variability in the location of the volcanoes along the arc (see **Figure 2B**) may be explained by the non-uniform dip of the slab below Sumatra (Hall and Spakman, 2015). To test this possibility, we compare the location of the volcanoes to the mean depth of the slab below them. In particular, the distribution of the volcanoes as a function of the distance from this mean depth of the slab at 130 ± 20 km, as well as from the GSF, is reported in **Figure 3**. In **Figure 3** the mean depth of the slab at 130 km coincides with the 0 km depth on the X-axis. This figure shows that a part of the volcanoes clusters at the mean depth of the slab (slab depth-controlled dashed line), while a part clusters at a minimal distance from the GSF (GSF-controlled dashed line). However, a significant amount of volcanoes lies in between the two dashed lines, suggesting a location independent of both the GSF and the depth to the slab. This distribution implies that other mechanisms, in addition to the slab depth and the location of the GSF, may determine the location of the volcanoes in Sumatra.

In order to understand more in detail the distribution of the volcanoes with regard to the location of the GSF, we first extract the volcanoes lying above a shallower or deeper slab (i.e., slab depth $z \leq 115$ km or >145 km, respectively, which represent the 20$^{th}$ and 80$^{th}$ percentiles of the distribution of the depth of the slab in the dataset); the location of these volcanoes may be partly controlled by factors different from the slab depth, such as a local weakness caused by the GSF (**Figure 4A**). We then compare the distribution of the distances of these volcanoes from the GSF to the distance of all the other volcanoes from the GSF, considering that, in case the position of the former volcanoes is GSF-controlled, their distance should be significantly smaller than the one of the latter group. We test such possible difference by means of two nonparametric statistical tests, i.e., the Kolmogorov-Smirnoff two-sample test and the Mann-Whitney-Wilcoxon test (Hollander and Wolfe, 1973). In particular, the former test compares the Empirical Cumulative Distribution Functions (ECDF) of the distance volcano-GSF in the two groups (see **Figure 4B**), under the null hypothesis that they are two independent samples drawn from the same continuous distribution; the latter test is for equality of two samples' medians. The tests on the distance between volcanoes and the GSF in the two groups show that: (1) in the case of volcanoes overlying deeper slabs, the distribution of their distances from GSF is significantly different, and in particularly takes much larger values than the ones of the other volcanoes; this excludes a control of GSF on their positioning; (2) in the case of volcanoes overlying shallower slabs, there is no statistical difference: in particular, both the Kolmogorov-Smirnoff two-sample test and

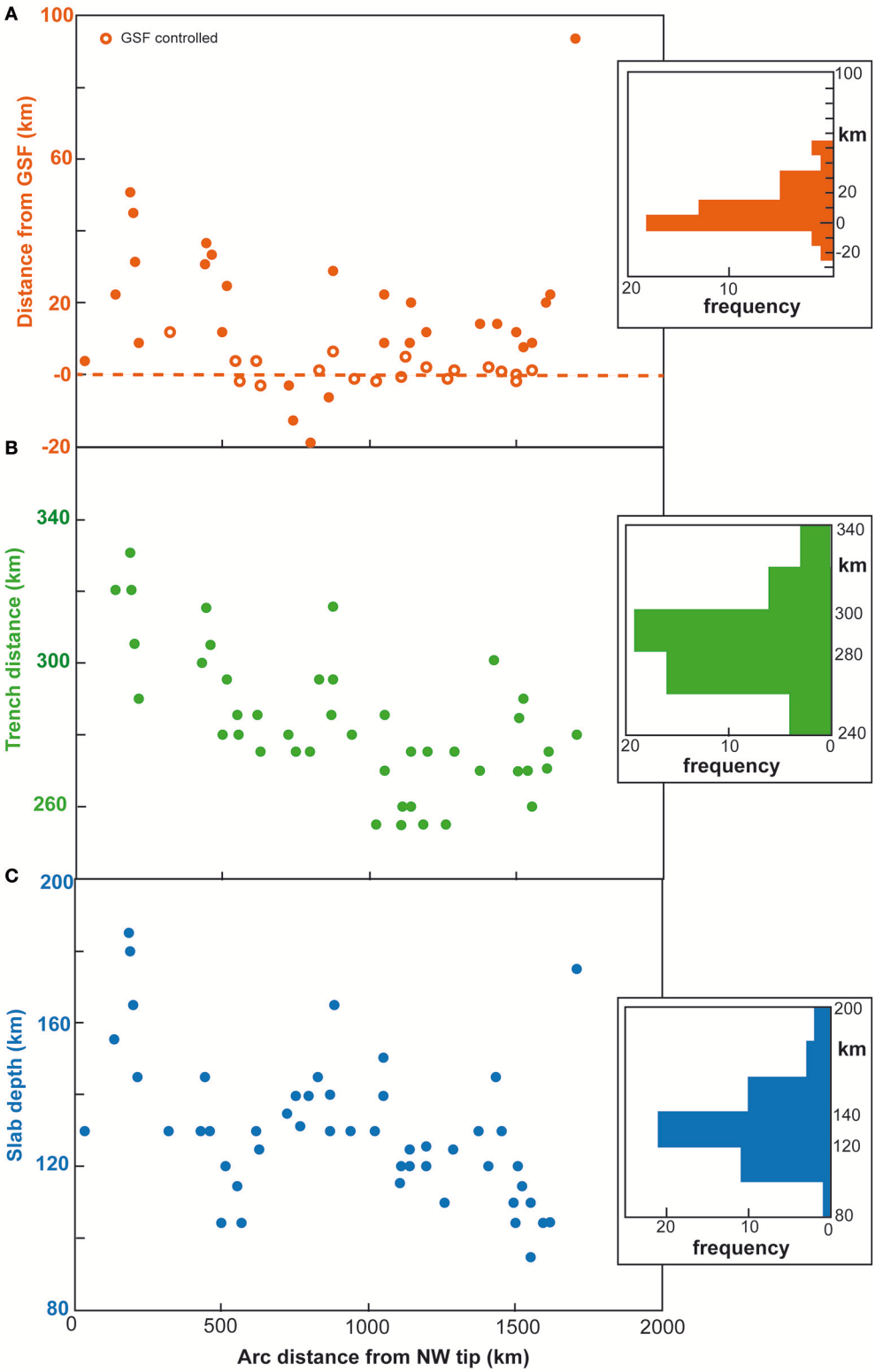


**FIGURE 2 |** Distribution of volcanoes along Sumatra (from NE, to the left, to SW, to the right) as a function of the distance from GSF **(A)**, from the trench **(B)** and as a function of the slab depth **(C)**. Empty circles in **(A)** highlight the 19 volcanoes which may be related to the GSF activity, according to the conditions described in **Table 1** ("GSF tectonic control").

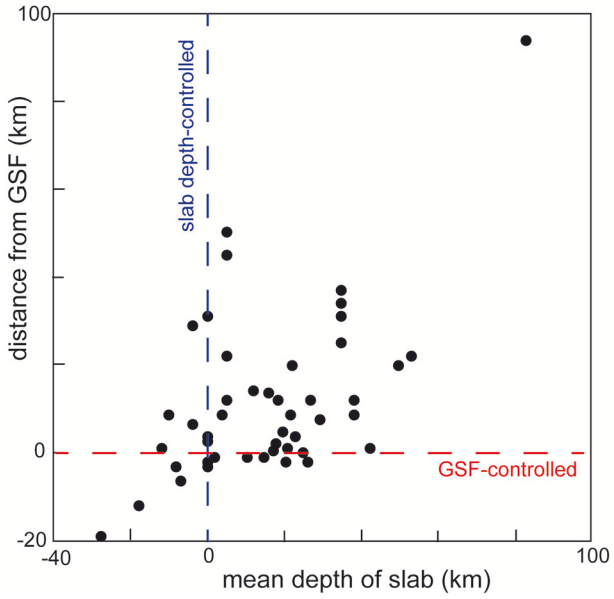


**FIGURE 3 |** Distribution of volcanoes as a function of the mean depth of the slab (considering a reference of 130 km, see **Figure 2C**) and of the GSF. See text for details.

the Wilkocoxon-Mann-Whitney test provide $p$-values > 5%, highlighting no significant differences in the shape/tails and in the median of the ECDF of the volcanoes-GSF distance, respectively, in the two groups of volcanoes. This implies that the location of volcanoes above slabs at different depths has no evident relationship with their proximity to the GSF. **Figure 4A** also shows that volcanoes within the NW half of Sumatra are generally farther away from the fault with respect to the ones within the SE half. We look for potential differences in the ECDF of the distance volcano-GSF in these two portions of the GSF (**Figure 4C**); in this case, this difference is confirmed both by means of the Kolmogorov-Smirnoff two-sample test and the Wilkocoxon-Mann-Whitney test ($p$-values < 1% in both cases). This difference confirms that there is an overall closer spatial relationship between the volcanoes and the GSF in the southern half of Sumatra.

Of the 25 volcanoes (46% of population) lying within 10 km from the GSF, only 7 (28%) have an evident structural relationship with the configuration of the fault segments of the GSF. These volcanoes are in fact located within pull-apart or releasing bend zones formed by offset dextral segments, and it is likely ("likely control") that here the rise of the magma may have been associated with the local extension created by the activity of nearby GSF structures. Other 12 volcanoes (48% of data) also lie along major splays of the GSF, even though their location with regard to areas of localized extension is uncertain: overall, these volcanoes show a "probable" to "possible" structural control of the GSF. The reminder 6 volcanoes (24% of data) lie outside the major splays of the GSF and thus do not have any evident structural connection with the latter; while we cannot discard any structural control of the GSF, this appears unlikely.

**Figure 5** shows three examples of possible structural control of the 19 volcanoes found along the GSF (**Figure 2A**; **Table 1**). In particular, the figure shows an example of volcano located with an area of localized extension, very likely controlled by the GSF structure (a; pull apart-releasing bend in **Table 1**), between two major splays of the GSF (b; probable link to GSF) and along the GSF (c; possible link to GSF). We recall that our analysis regards the present-day structure of the GSF, without considering its recent evolution and modifications, also in terms of segment interaction and linkage. On the one side, this implies that some of the volcanoes, even large calderas, may have been located, during their formation, along localized areas of extension (releasing bends, pull-aparts) between strike-slip segments which may have presently been partly obliterated by their linkage. On the other side, several features suggest that this limitation may not be really significant for this study, as: (a) the lifespan of the active stratovolcanoes should be in the order of a very few tens of thousands of years, similar to other volcanic edifices worldwide; (b) over such time spans, the overall architecture of the GSF is expected not to change dramatically, nor to obliterate previously formed structures (as releasing bends or pull-aparts); (c) it is unlikely that volcanoes distant from the GSF (>20 km) were controlled by the GSF in the past more than they are now. These features suggest that any variation in the geometry of the GSF in the last tens of thousands of years should not have produced significant variations in the structural control of the volcanoes.

As far as the productivity of the volcanic arc is concerned, there is an overall similar estimated erupted budget along the island, with the evident exception of Toba (**Figure 6A**). Even though the volumes of Toba are DRE, assuming a first-order but likely correction of 0.5 for the non-DRE equivalent (e.g., Rose and Chesner, 1987), the obtained value is still 1-2 orders of magnitude larger than that of the other Sumatran volcanoes. This exceptional productivity can be explained by the presence of a tear in the slab below Toba (Fauzi et al., 1996; Hall and Spakman, 2015). The volcanoes with an evident or possible link to the GSF do not usually show the highest erupted volumes, suggesting that the structural setting may enhance the location of a volcano, but not its longer-term production. The diagram in **Figure 6A** also shows the known longer-term (geological) slip rates along the GSF; with the exception of the northern tip of Sumatra, there is an overall southward decrease in the slip rate of the segments of the GSF, from 38 to 5.5 mm/year. There is no significant correlation between the variation of the erupted volumes along the arc and the known slip rates of the GSF (visually from **Figure 6B**, and quantitatively by means of a significance test on the Spearman correlation coefficient), both including and excluding Toba caldera from the test; therefore, the similar erupted volumes along Sumatra suggest that the volcanic productivity does not depend upon the activity (slip rate) or the crustal structures. The only exception may be Toba. However, because Toba is an isolated case, the highest slip rates in the northern part of Sumatra should not be considered to impact the highest erupted budget on Toba.

We finally consider the productivity of the arc volcanoes as a function of the obliquity of convergence. In fact, previous studies suggested a possible correlation between the amount

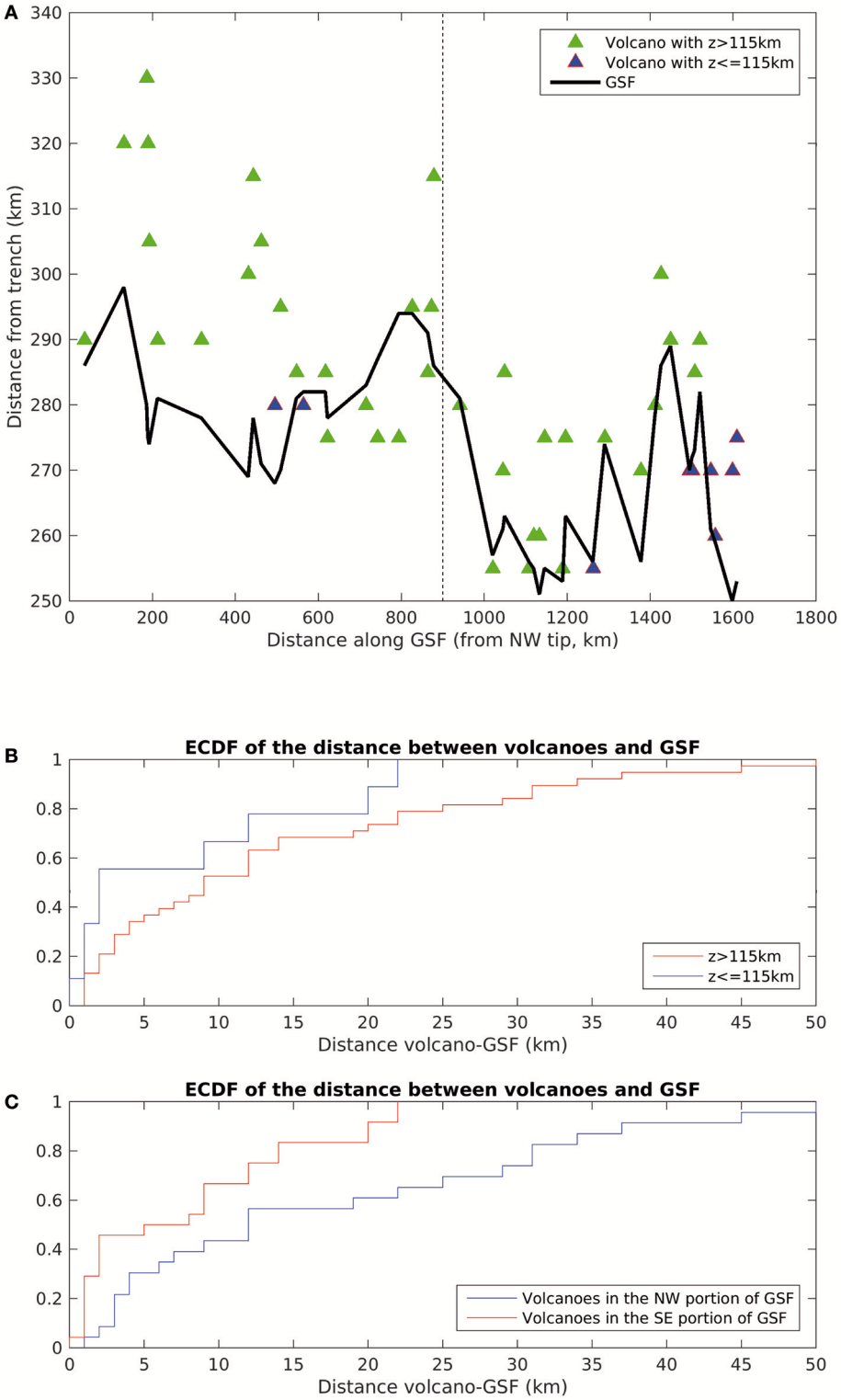


**FIGURE 4 | (A)** Distance of the GSF (black line) and of the Sumatran volcanoes (green triangles), also characterized by a shallower depth z of the slab (in blue), from the trench; the dashed vertical line divides the NW portion of the island from the SE portion. **(B)** ECDF of the distance between the volcanoes and the GSF, considering the depth of the slab z ($z > 115$ km and $z \leq 115$ km); **(C)** ECDF of the distance between the volcanoes and the GSF, considering the location of the volcanoes (NW or SE portion of Sumatra). See text for details.

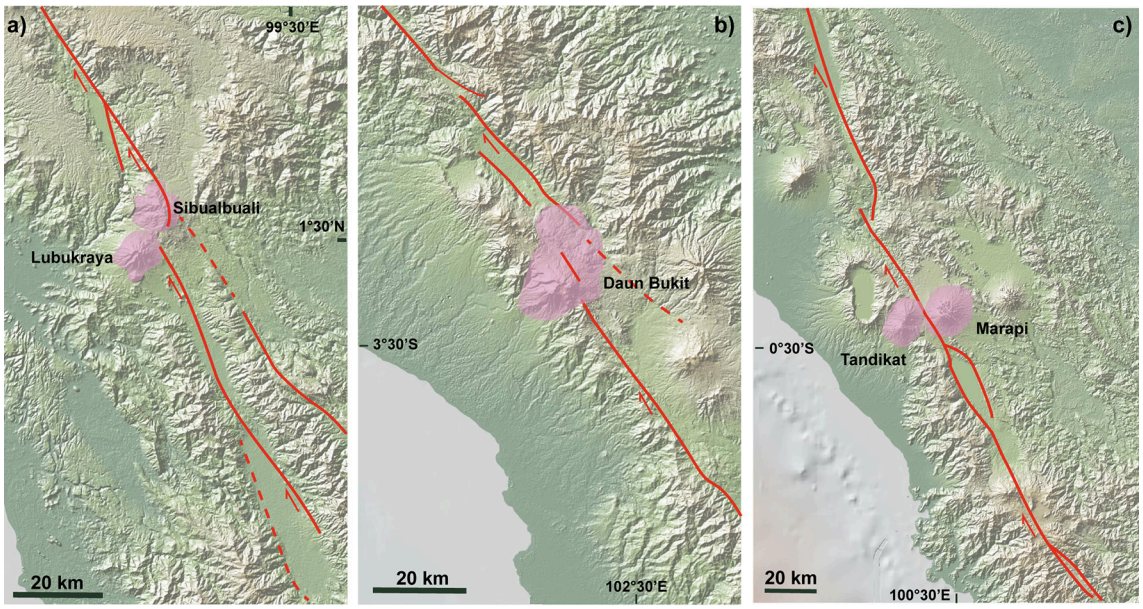


**FIGURE 5 |** Examples of volcanoes (purple areas) very likely **(a)**, probably **(b)**, and possibly **(c)** controlled by the GSF structures (red lines; dashed when inferred). Schematic GSF structure taken from Sieh and Natawidjaja (2000).

of arc-parallel convergence and the erupted volumes along the Sumatra Arc (Bardintzeff et al., 2000; Bellier et al., 2000). To this aim, we considered the ratio between the amount of convergence parallel to the arc (Vcp) and that orthogonal to it (Vcn), as previously calculated for six portions of the Sumatra arc (Heuret and Lallemand, 2005; Lallemand et al., 2005) and compared this to the estimated erupted volumes (**Table 2**) for the same arc portions. The results show that there is a significant linear correlation ($R^2 = 0.86$, $p$-value = 3%) between the amount of obliquity and the magmatic productivity when including Toba (**Figure 6C**), even though such relationship disappears when excluding the volume erupted by Toba (white circle in **Figure 6C**). Considering Toba confirms that the larger is the amount of arc-parallel convergence along Sumatra, the larger is the magmatic productivity.

There is also a significant positive correlation ($\rho_{Spearman} = 0.35$, $p$-value = 2%; **Figure 7A**) between the volume erupted by the volcanoes and the depth of the slab beneath them: generally, the deeper the slab, the larger the erupted volume. This may be explained by the fact that a higher percentage of fluids may be released from the slab at higher depths, also depending on the thermal state of the slab (Reynard, 2016). Two further significant correlations are found. A first one ($\rho_{Spearman} = 0.43$, $p$-value < 1%; **Figure 7**) between slip rate along the GSF and the distance of the GSF from the trench: the farther the GSF from the trench, the faster it slips. This may be explained by the fact that strain partitioning on the overriding plate may be more effective when the strike-slip domain lies farther from the trench. The other correlation ($\rho_{Spearman} = 0.47$, $p$-value < 1%; **Figure 7**) is found between the slip rate along the GSF and the distance between the volcanoes and GSF: the faster the GSF slips, the farther the volcanoes are from the GSF. We do not have any specific explanation for this behavior, and look forward for its confirmation and better understanding with other cases elsewhere.

The spacing of the volcanoes along a distance parallel to the arc highlights an overall asymmetric long-tailed distribution, peaking at a distance between 10 and 20 km (**Figure 8A**). A partly similar distribution, even though with two distinct peaks probably related to the minor amount of data, was previously described; indeed, our asymmetric long-tailed distribution is consistent with that of other volcanic arcs, and may reflect the repeated reactivation of plumes pathways at depth (de Bremond d'Ars et al., 1995).

Both the volcano elongation and the vent alignment peak in correspondence of NNE-SSW to NE-SW trends (**Figures 8B,C**), parallel or subparallel to the convergence vector. However, while the peak is evident in the vent alignment, the elongation of the volcanoes shows a larger scatter, with subordinate NNW-SSE to NW-SE orientations. These are parallel or subparallel to the GSF trend, suggesting a control of the faults on the elongation of some volcanoes. No evident across-arc variation of the volcano elongation or vent alignment has been observed.

Finally, despite the elongation and alignment of volcanoes, any evident continuation of the volcanic field outside the main volcanic edifice, through aligned monogenetic cones, has not been observed or reported on Sumatra; in fact, volcanic activity remains largely confined within the stratovolcanoes.

## The Structural Data

The structural data consist of a set of faults measured at several sites along and immediately to the side of the GSF, along its major splays. These faults are well developed at the outcrop scale and accompanied by widespread tectonic breccia; these structures

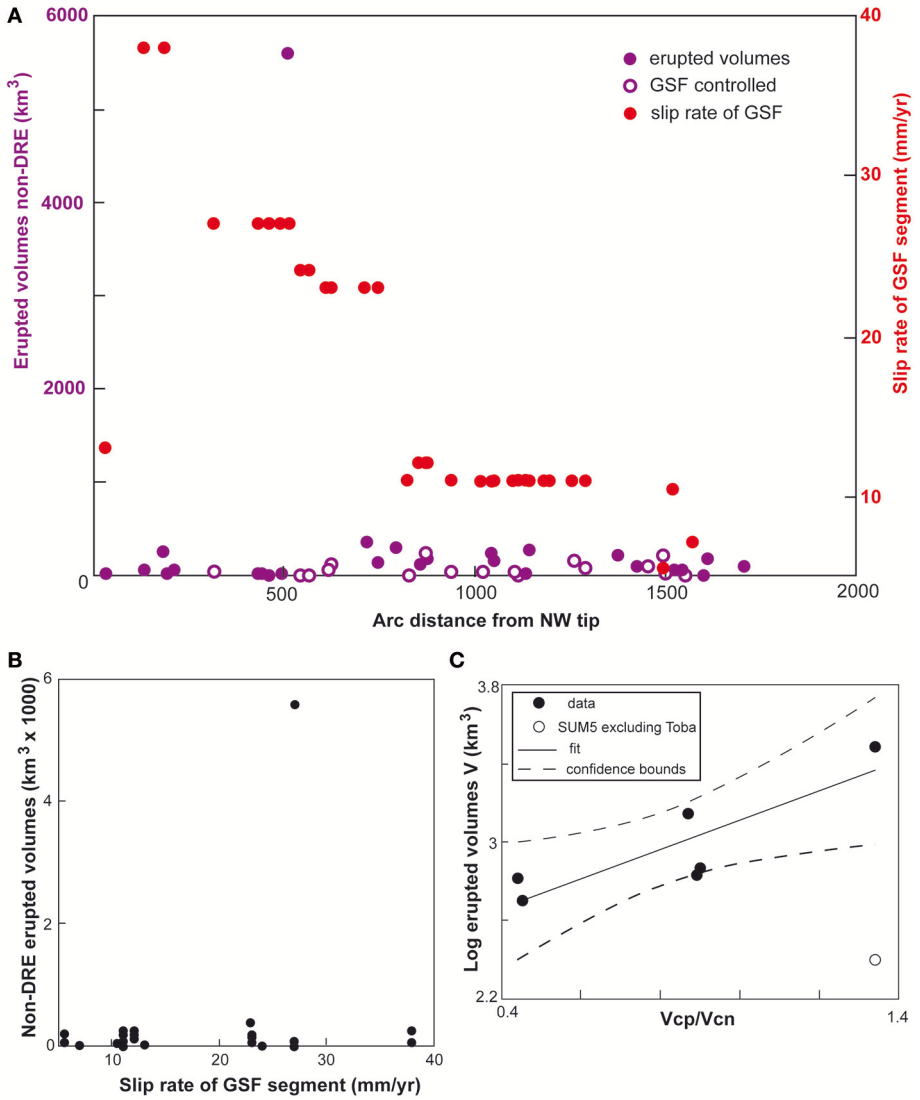


**FIGURE 6 | (A)** Non-DRE (except for Toba) erupted volumes and GSF slip rates along the Sumatra arc; **(B)** GSF fault slip vs. non-DRE erupted volumes at Sumatra; **(C)** Log of non-DRE erupted volumes as a function of the obliquity of convergence, expressed as the ratio between the amount of parallel convergence (Vcp) and that of orthogonal convergence (Vcn); see text for details.

also lie in correspondence of active fault traces observed on remote sensing data (satellite images and DEMs), underlying their importance at a wider scale. These features suggest that these faults are important splays of the GSF, with possible displacement in the order of tens to hundreds of meters. The structural field data are illustrated in **Figure 9** (central GSF) and **Figure 10** (southern GSF). These data have been grouped into plots summarizing the reconstructed structural evolution of each area, based on cross-cutting relationships among faults with different strike and kinematics, and among different striations (pitch values) on the same fault plane. As far as the central part of the GSF is concerned, the structural data have been collected along the main splays of the GSF, with the exception of site 1, within Quaternary deposits (volcano sedimentary, alluvial fans, fluvial). While some data (plots A, C and, partly E) show a predominance of NNW-SSE striking faults parallel to the GSF, others (plots D, B and, partly, E) show that WNW-ESE striking fault systems may locally predominate. These two main trends are also highlighted in the strike distribution of the faults reported in **Figure 11A**, peaking at ∼N-S and ∼WNW-ESE directions. From a kinematic point of view, the NNW-SSE striking systems show extensional to dextral transpressional motions (plots A, C and E; **Figure 9**); conversely, the WNW-ESE faults show both a dextral (these faults usually have a more NW-SE direction and higher dip; plot D, **Figure 9**) and reverse displacements (these faults usually have a more E-W direction and lower dip; plot B, **Figure 9**). The variability in the kinematics of the faults is also expressed by the distribution of

**TABLE 2 |** Location (lat., long. and width), velocity of convergence (total convergence Vc, normal and parallel convergences, Vcn and Vcp, respectively, all in mm/yr) and erupted volumes (see **Table 1**) of segments of the volcanic arc of Sumatra, as proposed in Heuret and Lallemand (2005) and Lallemand et al. (2005).

| Arc Segment | Lat. | Long. | Width (km) | Vc (mm/year) | Vcn | Vcp | Vcp/Vcn | Volumes ($km^3$) |
|---|---|---|---|---|---|---|---|---|
| *SUM6* | 2 | 95 | 367 | 45 | 41 | 18.3 | 0.45 | 502.6 |
| *SUM5* | 0 | 97 | 315 | 47 | 28 | 37.5 | 1.34 | 246/3046 |
| *SUM4* | −2 | 98.1 | 265 | 49 | 37 | 32.1 | 0.9 | 1,395.7 |
| *SUM3* | −4 | 99.7 | 290 | 51 | 38 | 34.1 | 0.9 | >742 |
| *SUM2* | −5.5 | 100.8 | 239 | 52 | 39 | 34.8 | 0.89 | >682.2 |
| *SUM1* | −7 | 102.3 | 349 | 54 | 50 | 21.9 | 0.44 | 646.9 |

*See text for details.*

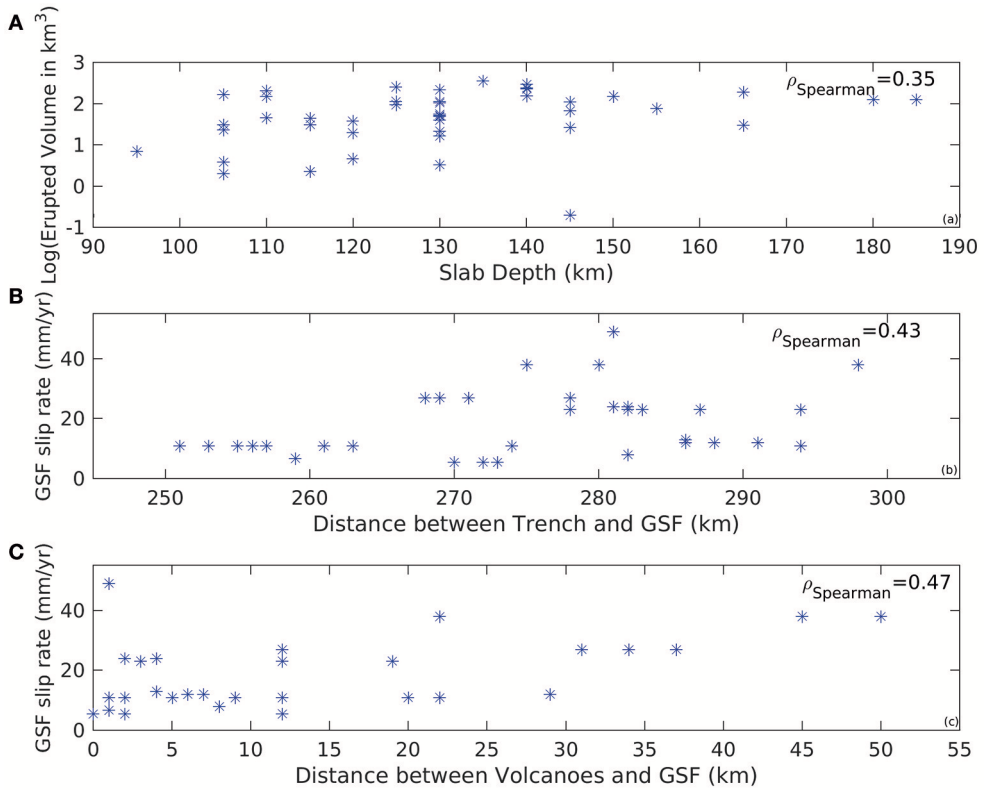


**FIGURE 7 | (A)** Log of the erupted volumes along the Sumatra arc as a function of the slab depth; **(B)** Slip rate of the GSF as a function of the distance between the trench and the GSF. **(C)** Slip rate of the GSF as a function of the distance between the volcanoes and the GSF. See text for details.

the pitch values of the faults (**Figure 11B**). These peak in the dip-slip domain (associated to both normal and thrust faults), as well as in the oblique and strike-slip (dextral) domain. These faults indicate that along the dextral GSF, in addition to the NW-SE striking dextral splays, the deformation pattern may be complicated by ∼N-S striking normal faults and WNW-ESE striking thrust faults. The inversion of the structural data highlights a ∼WNW-ESE extension direction, associated with a NNE-SSW direction of maximum compression (**Figure 9**), suggesting the GSF kinematics varies between transtension and transpression.

The structural data along the southernmost part of the GSF have been collected in the Semangka Bay area, where the right-lateral GSF terminates offshore on a set of normal-fault grabens within the Sunda Strait (**Figure 10**). These data have been collected at 7 outcrops and in 3 trenches, the latter all along the GSF, within Neogene to Holocene deposits (volcano sedimentary, alluvial fans and colluvial deposits, sandstones). A first compressional event was characterized by a ∼N-S trending maximum horizontal compression, associated with a subvertical (contractional domain; plot F; **Figure 10**) or a subhorizontal minimum compression (strike-slip domain; plot G; **Figure 10**). In both cases, predominant NNW-SSE striking dextral faults are activated. This compressional kinematics was followed by two extension directions: an arc-normal extension, mainly activating NW-SE striking normal faults (plot H; **Figure 10**), followed by

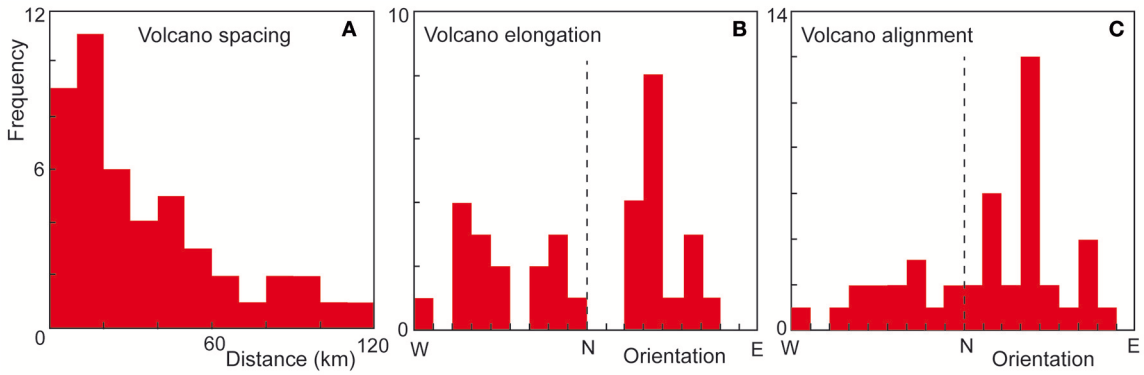


**FIGURE 8 | (A)** Spacing, **(B)** orientation (from west to east) of the elongation and **(C)** alignment of the volcanoes along the Sumatra arc.

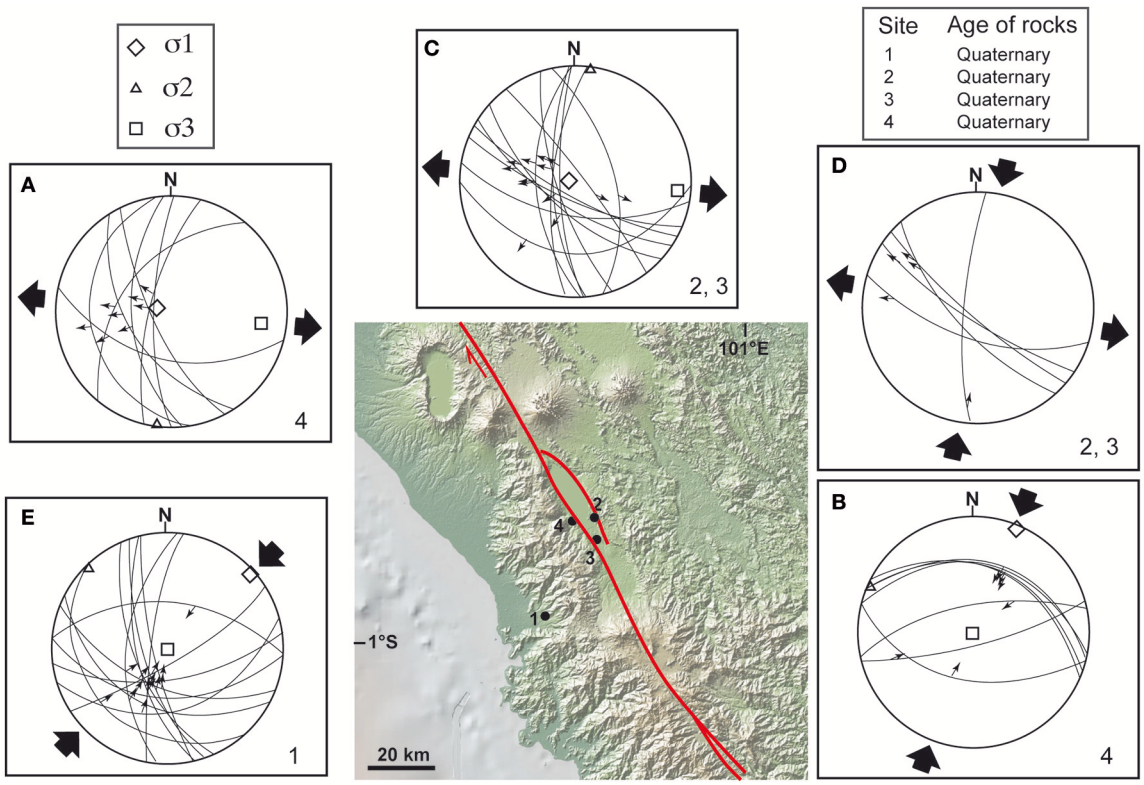


**FIGURE 9 |** Overview of the collected structural field data, along the central portion of the GSF, on lower hemisphere stereograms of fault slip data together with the inversion results characterizing stress regimes. Numbers at bottom right of stereograms refer to the sites where the structural data have been measured (location in the map). Letters at upper left of stereograms (from **A** to **E**) are used as reference in the text. The used inversion method (e.g., Carey, 1979) assumes that the slip represented by the striation occurs in the direction of the resolved shear. Deviatoric principal stress axes: $\sigma_1$, $\sigma_2$, $\sigma_3$, are the compressional, intermediate and extensional deviatoric axes, respectively. The age of the faulted formation is also reported. The exact location for the deviatoric principal stress axes could not be determined in **(D)** because of the relatively few (five) and clustered (four out the five) data.

an arc-oblique (WNW-ESE striking) extension, mainly activating NNW-SSE dextral transtensive faults (plot I; **Figure 10**). As the fault slip data of the latter event are seen both at the contact and within the Holocene deposits, the NNW-SSE transtensive dextral faults correspond to the present-day kinematics. Most of the collected faults in the southernmost part of the GSF have a NNW-SSE strike (**Figure 11C**), and are associated to both dextral and normal motions (**Figure 11D**); however, the highest peak in the pitch distribution is given by a moderately positive dip-slip motion (**Figure 11D**); as most faults have a NE plunge, this peak reflects the previously mentioned dextral transtensive kinematics.

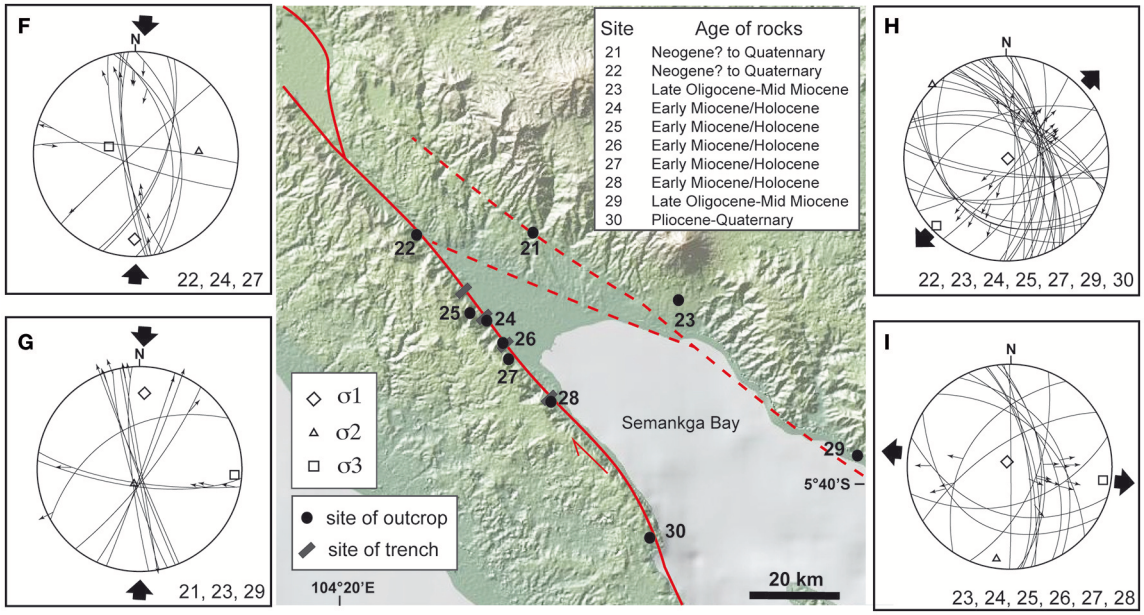


**FIGURE 10 |** Overview of the collected structural field data, along the southern portion of the GSF, on lower hemisphere stereograms of fault slip data together with the inversion results characterizing stress regimes. Numbers at bottom right of stereograms refer to the sites where the structural data have been measured (location in the map). Letters at upper left of stereograms (from **F** to **I**) are used as reference in the text. The used inversion method (e.g., Carey, 1979) assumes that the slip represented by the striation occurs in the direction of the resolved shear. Deviatoric principal stress axes: $\sigma_1$, $\sigma_2$, $\sigma_3$, are the compressional, intermediate and extensional deviatoric axes, respectively. The age of the faulted formation is also reported.

Overall, the collected structural data highlight a present-day stress regime with a ~NNE-SSW trending direction of maximum compression, responsible for compressive structures to the west of GSF (plot B; **Figure 9**) and for NNW-SSE to NW-SE striking dextral (plots F and G; **Figure 10**) or normal faults (plots A, C, H and I; **Figures 9**, **10**) along the GSF, in broad accordance with previous studies; the normal faults extend with a ~WNW-ESE trend and, subordinately, NE-SW one (Bellier and Sébrier, 1994).

## DISCUSSION

Most of the GSF consists of a very few km wide zone of deformation along a main dextral segment (Sieh and Natawidjaja, 2000), vertical down to at least 15 km, at the bottom of the brittle crust (Weller et al., 2012). This implies that volcanoes at distances >20 km from any GSF segment should not be controlled by its activity. As nearly one third of the considered volcanoes lies at >20 km from the GSF, it is possible to exclude any "structural control" of the fault zone (**Figure 2**); by means of "structural control" we refer here to the definitions previously given in section General Tectono-Magmatic Features of the Arc. However, a significant part of the volcanoes lies in proximity (<20 km) to the GSF. As anticipated, any possible control of the GSF on the location of these volcanoes may be biased by the maturity of the GSF. In fact, the southern propagation and overall evolution of the GSF, affecting the interaction and linkage of its segments, may modify the localized areas of extension created by the activity of offset dextral segments and possibly promoting the development of the volcanoes. This evolution may partly explain why most of the volcanoes (nearly half of them), even though lying along the GSF, do not appear to be clearly structurally-controlled, so that any relationship to the GSF may be questioned. However, all together, the spatial distribution of the volcanoes in Sumatra, as summarized in **Figures 2**–**4**, suggests a possible, even though anyway limited, structural control of the GSF. This limited structural control may be also supported by the evidence that the erupted volumes seem independent of the presence and activity (slip rate) of the GSF (**Figure 6**), and that the highest magmatic productivity at Toba may be explained by a tear in the slab beneath.

Overall, these data point out a limited role of the strike-slip structures on volcanism at Sumatra. This somehow contrasts with previous evidence from the deeper structure of extinct and eroded magmatic arcs, where pluton emplacement has been commonly associated with local extension created by strike-slip systems (Acocella and Funiciello, 2010, and references therein). This may be explained by a different structural control of the magmatic arc at depth and at the surface, with a decoupling in the tectono-magmatic relationships responsible for a stronger structural control on magma emplacement at depth and a weaker control on the rise of the magma at the surface; a similar behavior has been postulated for the central Aeolian Arc (Ruch et al., 2016). Another possibility to explain the apparently more limited structural control on the Sumatra arc compared to other eroded arcs may be related to the different timing in the development of the GSF along the island. In fact, the more recent central-southern portion of the GSF formed in the last 2 Ma

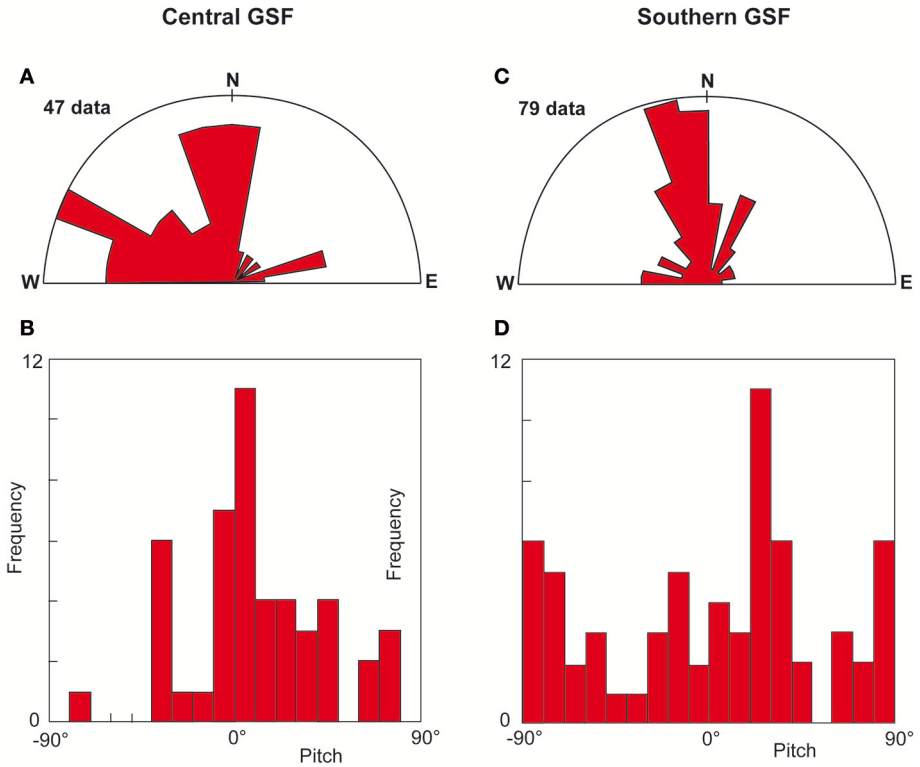


**FIGURE 11 |** Distribution of the strike **(A)** and pitch **(B)** of the collected faults shown in **Figure 7** (central GSF; **A,B**) and in **Figure 8** (southern GSF; **C,D**). Here we use the convention that pitch values range from −90° to +90°; these correspond to pure strike-slip motions, whereas pitches = 0° correspond to pure dip-slip motions.

(Sieh and Natawidjaja, 2000), thus postdating the older Miocenic volcanism. The fact that the latter, especially south of Toba, is broadly found in the same location as the Quaternary volcanism (Rock et al., 1982) indicates that the Miocenic arc was not controlled by the GSF and suggests that a similar condition may apply also to the Quaternary arc in central-southern Sumatra. Indeed, the location of the GSF along this part of the volcanic arc suggests that the focusing of the strain in the upper plate has been promoted by the magma-induced thermal weakening of the crust. In the southern half of Sumatra there is still a closer spatial relationship of the volcanoes with the GSF (**Figure 4C**); this implies that the magma-induced thermal weakening of the crust may be an effective means to localize the crustal deformation in correspondence of the volcanic arc.

While the development of a minor part of volcanoes may be explained by the activity of the GSF, the development of the remainder, forming most of the population, may be explained by more general tectonic processes. These may include the mean depth of the slab (130 ± 20 km) and, subordinately, the extension along the GSF.

The mean depth of the slab holds regardless of the distance from the trench, implying a variable dip of the slab. The general control of the arc front by the corner location of the asthenospheric wedge was previously inferred for Sumatra (Bellier and Sébrier, 1994; Bellier et al., 1999) and is also consistent with what previously observed elsewhere, as for example in the Peruvian Andes (Sébrier and Soler, 1991). In addition, here we observe that the deeper the slab, the larger the erupted volumes (**Figure 7A**), suggesting that a higher percentage of fluids may be released from the slab at higher depths. Moreover, there is a proportional relationship between the variations in the arc-parallel convergence and the related erupted volumes, confirming previous studies (**Figure 6C**; Bardintzeff et al., 2000; Bellier et al., 2000). Such a relationship does not have an evident explanation, and may be biased by the much higher erupted volumes from Toba.

The extension along the GSF, where ∼WNW-ESE oriented, may result from localized extension among GSF segments, especially in the areas where oversteps are present, or from the overall tectonic convergence. This WNW-ESE extension direction, perpendicular to the convergence vector (**Figure 12A**), is suggested by the collected structural field data in the central and southern part of the GSF (**Figures 9**, **10**) and is also supported by structural and geophysical studies (Lassal et al., 1989; Harjono et al., 1991; Pramumijoyo and Sébrier, 1991; Mount and Suppe, 1992; Kundu et al., 2012; Muksin et al., 2014). The ∼WNW-ESE extension direction may explain the common ∼NNE-SSW elongation and/or alignment of many volcanoes (**Figure 8**). Another cluster in the elongation of volcanoes is along the NNW-SSE to NW-SE trends, subparallel to the GSF structures. This parallelism may be explained by the presence of major extension along the GSF, as also supported by the collected

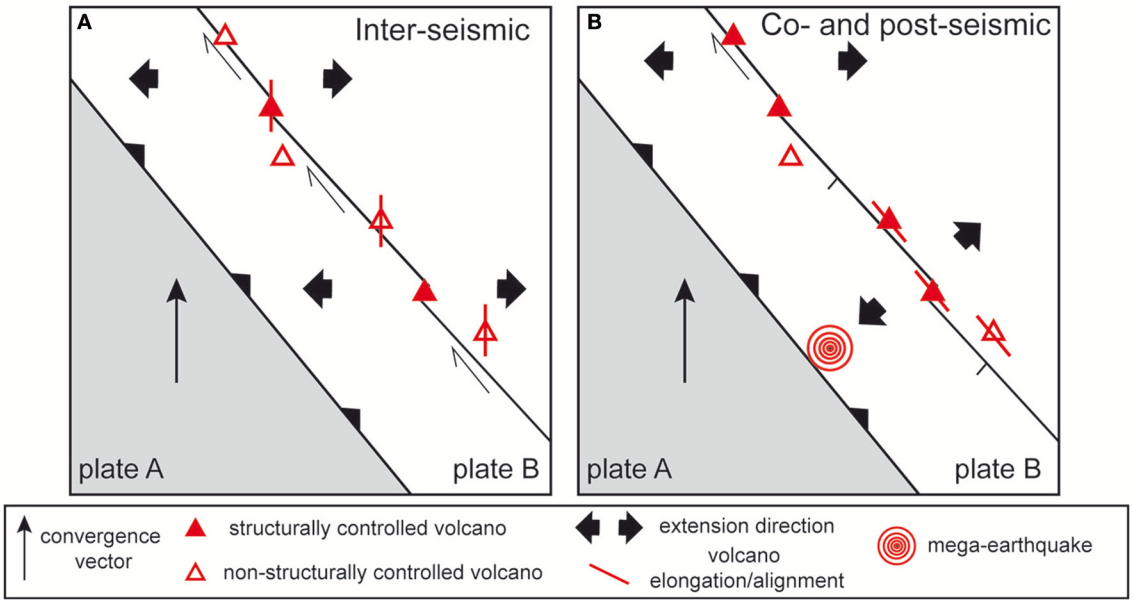


**FIGURE 12 |** Summary of the possible tectono-magmatic conditions along an obliquely convergent volcanic arc. **(A)** Normally, as during the inter-seismic period, the arc is characterized by the activity of strike-slip (dextral, in this case) structures associated with strain partitioning; part of these structures control the location of the volcanoes ("structurally controlled volcano"); the location of other volcanoes ("non-structurally controlled volcano") away from the strike-slip zone may be explained by other processes, as slab depth or convergence-orthogonal extension, controlling also volcano alignment and elongation. **(B)** During transient periods (co- and post-seismic periods due to the activity of mega-earthquakes) the arc may undergo arc-normal extension, with the local reactivation of the strike-slip faults as normal faults; the alignment and elongation of volcanoes may partly reflect these transient conditions, becoming subparallel to the arc.

structural data, showing NE-SW trending extension along NW-SE to N-S striking faults, especially to the south (**Figure 10**). The presence of such an arc-normal extension along the GSF is not straightforward, as the GSF clearly has a predominant strike-slip component, with limited vertical offset (e.g., Bellier et al., 1997; Genrich et al., 2000; Prawirodirdjo et al., 2000; Sieh and Natawidjaja, 2000). One possible explanation for this local arc-normal extension along the GSF may be related to the occurrence of mega-earthquakes along the subduction zone, capable of promoting transient stress variations in the upper plate (**Figure 12B**). In fact, while in the inter-seismic period the kinematics of GSF may be predominantly dextral, in the co- and (to a lesser extent) post-seismic cycle the arc may experience significant arc-normal extension. This has been observed not only after the 2004 Sumatra mega-earthquake (Subarya et al., 2006; Gahalaut et al., 2008; Shearer and Burgmann, 2010), but also in NE Japan after the 2011 Tohoku mega-earthquake (Ozawa et al., 2011; Simons et al., 2011; Takada and Fukushima, 2013) and in Southern Chile after the M9.5 1960 and the M8.8 2010 Maule mega-earthquakes (Barrientos and Ward, 1990; Wang et al., 2007; Vigny et al., 2011; Pritchard et al., 2013). In the latter two cases, mega-earthquakes promoted the transient (co- and post-seismic) inversion of the major tectonic structures, also affecting magmatic activity (Singer et al., 2008; Takada and Fukushima, 2013). Another possibility to locally explain the arc-normal extension may be related to the pressurization promoted by the intruded magma along the arc. A similar mechanism has been proposed to explain the widespread and consistent extensional structures on the central Aeolian Arc (Ruch et al., 2016), inferred to experience strike-slip motions at depth (De Astis et al., 2003). However, such a possible shallow tectonic reorganization does not appear completely feasible for the Sumatra Arc. In fact, here volcanic activity is largely confined within the largest edifices, suggesting the lack of developed elongated magmatic systems. Indeed, this feature on Sumatra implies a punctiform, not linear, mode of rise of the magma in the crust, similarly to what observed along other magmatic arcs not experiencing extension, as the contractional arc of NE Japan (Acocella et al., 2008). Conversely, along the central Aeolian Arc there is evidence of magmatism continuing, through eruptive fissures, outside the main volcanoes, suggesting the activity of magma-controlled magmatic systems. We thus propose that the development of the volcanoes elongated and aligned parallel to the GSF, as well as the collected structural data showing extension along the NW-SE to N-S trending structures, may be mainly controlled by transient stress variations promoted by mega-earthquakes, responsible for limited extension along the Sumatra arc (**Figure 12**).

Therefore, this study highlights a limited structural control on volcanism along obliquely convergent arcs experiencing strike-slip motions, even though this may reflect local, shallower crustal conditions. This feature is somehow intermediate between those observed in extensional arcs, where magmatism couples with the structure of the arc (as along the Taupo Volcanic Zone; Acocella et al., 2003) and shows shallow magma reservoirs (Chaussard and Amelung, 2012) and those in contractional arcs,

where the arc configuration is largely independent of the shallow structural features (as in NE Honshu, Japan; Acocella et al., 2008). However, the overall lack of magmatic systems makes the strike-slip Sumatra arc more similar to the contractional ones.

## CONCLUSIONS

The available data along the volcanic arc of Sumatra suggest that the location and productivity of most volcanoes are not controlled by the activity of the dextral GSF. Rather, these features seem to be mainly controlled by the location of the depth of the slab beneath the island. Indeed, the asthenospheric wedge seems to control both the location of the volcanic arc (depth of partial melting, consistently with previous studies; Bellier and Sébrier, 1994; Bellier et al., 1999) and of the GSF (thermal contrast in the upper plate localizing the rheological weakness of the fault zone). More locally, the volcanic arc seems also controlled by a ∼WNW-ESE extension direction, orthogonal to convergence, which may explain the common ∼NNE-SSW elongation and/or alignment of many volcanoes (**Figure 12A**). There is also evidence of a subordinate arc-normal extension, as suggested by the collected structural data and the elongation of volcanoes, which may be related to a transient stress field active during the co- and post-seismic cycle induced by mega-earthquakes (**Figure 12B**). Overall, the strike-slip arc of Sumatra appears intermediate between extensional arcs, where magmatism couples with the arc structure and contractional arcs, where the arc configuration is largely independent of the shallow structure. However, the lack of magmatic systems (areas with focused monogenic magmatic and tectonic activity outside the main volcanic edifice) in Sumatra makes the strike-slip arcs more similar to the contractional ones.

## AUTHOR CONTRIBUTIONS

VA and OB: coordinated the work; VA: wrote the manuscript; LS: elaborated part of the data; OB, MS, and SP: collected the structural data. All authors discussed the results and contributed to writing the manuscript.

## ACKNOWLEDGMENTS

This study was carried under the frame of a cooperation program between CEREGE and Roma Tre, while VA was visiting professor at CEREGE. The previously unpublished structural field data were collected by Olivier Bellier and Michel Sébrier with Christine Detourbet and Subagyo Pramumijoyo. Two reviewers helped to significantly improve the manuscript.

## REFERENCES

Acocella, V. (2014). Structural control on magmatism along divergent and convergent plate boundaries: overview, model, problems. *Earth Sci. Rev.* 136, 226–288. doi: 10.1016/j.earscirev.2014.05.006

Acocella, V., and Funiciello, F. (2010). Kinematic setting and structural control of arc volcanism. *Earth Planet. Sci. Lett.* 289, 43–53. doi: 10.1016/j.epsl.2009.10.027

Acocella, V., Spinks, K., Cole, J., and Nicol, A. (2003). Oblique back-arc rifting of Taupo Volcanic Zone. New Zealand. *Tectonics* 22:1045. doi: 10.1029/2002TC001447

Acocella, V., Yoshida, T., Yamada, R., and Funiciello, F. (2008). Structural control on Late Miocene to Quaternary volcanism in the NE Honshu arc, Japan. *Tectonics* 27:TC5008. doi: 10.1029/2008TC002296

Allan, A. S. R., Wilson, C. J. N., Millet, M. A., and Wysoczansk, R. J. (2012). The invisible hand: tectonic triggering and modulation of a rhyolitic supereruption. *Geology* 40, 563–566. doi: 10.1130/G32969.1

Bardintzeff, J. M., Bellier, O., and Crochet, E. (2000). *Volcanic Production Rate and Oblique Convergence Associated to the Sumatran Subduction.* Bali: IAVCEI General Assembly.

Baroux, E., Avouac, J. P., Bellier, O., and Sébrier, M. (1998). Slip-partitioning and fore-arc deformation at the Sunda Trench, Indonesia. *Terra Nova* 10, 139–144.

Barrientos, S. E., and Ward, S. N. (1990). The 1960 Chile earthquake: inversion for slip distribution from surface deformation. *Geophys. J. Int.* 103, 589–598.

Beaudoin, T., Bellier, O., and Sébrier, M. (1995). Segmentation et alea sismique sur la Grande Faille de Sumatra (Indonesie). *C.R. Acad. Sci. Paris* 321, 409–416.

Bellier, O., Bardintzeff, M., and Crochet, E. (2000). "Productivitè volcanique et convergence oblique associèes a la subduction de Sumatra," in *Proceedings of the 18° Reunion des Sciences de la Terre La Villette* (Paris), 80–81.

Bellier, O., Bellon, H., Sebrier, M., Sutanto, P., and Maury, R. C. (1999). K-Ar age of the Ranau tuffs: implications for the Ranau caldera emplacement and slip-partitioning in Sumatra (Indonesia). *Tectonophysics* 312, 347–359.

Bellier, O., and Sébrier, M. (1994). Relationship between tectonism and volcanism along the Great Sumatra Fault Zone deduced by SPOT image analysis. *Tectonophysics* 233, 215–231.

Bellier, O., and Sebrier, M. (1995). Is the slip rate variation on the Great Sumatran fault accommodated by fore-arc stretching? *Geophys. Res. Lett.* 22, 1969–1972.

Bellier, O., Sébrier, M., and Pramumijoyo, S. (1991). La grande faille de Sumatra: geometrie, cinematique et quantitè de deplacement mises en evidence par l'imagerie satellitaire. *C.R. Acad. Sci. Paris* 312, 1219–1226.

Bellier, O., Sebrier, M., Pramumijoyo, S., Beaudouin, T.h., Harjono, H., Bahar, I., et al. (1997). Paleoseismicity and seismic hazard along the Great Sumatran Fault (Indonesia). *J. Geodyn.* 24, 169–183.

Bellier, O., and Zoback, M. L. (1995). Recent state of stress change in the Walker-Lane zone, Western Basin and Range Province, United States. *Tectonics* 14, 564–593.

Bradley, K. E., Feng, L., Hill, E. M., Natawidjaja, D. H., and Sieh, K. (2017). Implications of the diffuse deformation of the Indian Ocean lithosphere for slip partitioning of oblique plate convergence in Sumatra. *J. Geophys. Res.* 122, 572–591, doi: 10.1002/2016JB01354

Calais, E., d'Oreye, N., Albaric, J., Deschamps, A., Delvaux, D., Deverchere, J., et al. (2008). Strain accommodation by dyking in a youthful continental rift, East Africa. *Nature* 456, 783–787. doi: 10.1038/nature07478

Carey, E. (1979). Recherche des directions principales de constraintes assocciées au jeu d'une population de failles. *Rev. Geol. Dyn. Geogr. Phys*. 21, 57–66.

Carey, E., and Brunier, B. (1974). Analyse theorique et numerique d'une modele elementaire appliquè a l'etude d'une population de failles. *C.R. Acad. Sci. Set. D* 279, 891–894.

Catalan, N., Bataille, K., Tassara, A., and Araya, R. (2017). Depth-dependent geometry of margin-parallel strike-slip faults within oblique subduction zones. *Andean Geol.* 44, 79–86. doi: 10.5027/andgeoV44n1-a05

Cembrano, J., and Lara, L. (2009). The link between volcanism and tectonics in the southern volcanic zone of the Chilean Andes: a review. *Tectonophysics* 471, 96–113. doi: 10.1016/j.tecto.2009.02.038

Chaussard, E., and Amelung, F. (2012). Precursory inflation of shallow magma reservoirs at west Sunda volcanoes detected by InSAR. *Geophys. Res. Lett.* 39:L21311. doi: 10.1029/2012GL053817

Chesner, C. A. (2012). The Toba caldera complex. *Quat. Int.* 258, 5–18. doi: 10.1016/j.quaint.2011.09.025

Corti, G., Carminati, E., Mazzarini, F., and Garcia, M. O. (2005). Active strike-slip faulting in El Salvador, Central America. *Geology* 33, 989–992. doi: 10.1130/G21992.1

De Astis, G., Ventura, G., and Vilardo, G. (2003). Geodynamic significance of the Aeolian volcanism (southern Tyrrhenian Sea, Italy) in light

of structural, seismological, and geochemical data, *Tectonics* 22:1040. doi: 10.1029/2003TC001506

de Bremond d'Ars, J., Jaupart, C., and Sparks, R. S. J. (1995). Distribution of volcanoes in active margins. *J. Geophys. Res.* 100, 20421–20432.

DeMets, C. (1992). Oblique convergence and deformation along the Kuril and Japanese trenches. *J. Geophys. Res.* 97, 17615–17625.

De Silva, S. L., Mucek, A. E., Gregg, P. M., and Pratomo, I. (2015). Resurgent Toba—field, chronologic, and model constraints on time scales and mechanisms of resurgence at large calderas. *Front. Earth Sci.* 3:25. doi: 10.3389/feart.2015.00025

Detourbet, C. (1995). *Analyse des Relations entre la Grande Faille de Sumatra (Indonesie) et les Structures Compressives del l'arriere arc*. Ph.D. thesis, Universite de Paris-Sud, centre d'Orsay.

Detourbet, C., Bellier, O., and Sébrier, M. (1993). La caldeira volcanique de Toba et la Grande Faille de Sumatra (Indonesie) vues par l'imagerie SPOT. *C.R. Acad. Sci. Paris* 316, 1439–1445.

Duquesnoy, T.h., Bellier, O., Kasser, M., Sébrier, M., Vigny, C.h., and Bahar, I. (1996). Deformation related to the 1994 Liwa earthquake derived from geodetic measurements. *Geophys. Res. Lett.* 23, 3055–3058.

Ebinger, C. J., and Casey, M. (2001). Continental breakup in magmatic provinces: An Ethiopian example. *Geology* 29, 527–530. doi: 10.1130/0091-7613(2001)029<0527:CBIMPA>2.0.CO;2

Ego, F., and Ansan, V. (2002). Why is the Central Trans-Mexican Volcanic Belt (102°-99°W) in transtensive deformation? *Tectonophysics* 359, 189–208. doi: 10.1016/S0040-1951(02)00511-5

Fauzi, McCaffrey, R., Wark, D., Sunaryo, and Prih Haryadi, P. Y. (1996). Lateral variation in slab orientation beneath Toba caldera, northern Sumatra. *Geophys. Res. Lett.* 23, 443–446.

Fernandez-Blanco, D., Philippon, M., and von Hagke, C. (2016). Structure and kinematics of the Sumatran Fault System in North Sumatra (Indonesia). *Tectonophysics* 693, 453–464. doi: 10.1016/j.tecto.2016.04.050

Fossen, H. (2010). *Structural Geology*. Cambridge, UK: Cambridge University Press.

Gahalaut, V. K., Jade, S., Catherine, J. K., Gireesh, R., Ananda, M. B., Dileep Kumar, P., et al. (2008). GPS measurements of postseismic deformation in the Andaman-Nicobar region following the giant 2004 Sumatra-Andaman Earthquake. *J. Geophys. Res.* 113:B08401. doi: 10.1029/2007JB005511.

Gasparon, M. (2005). "Quaternary volcanicity." in *Sumatra: Geology, Resources and Tectonic Evolution,* Vol. 31, eds A. J. Barber, M. L. Crow, and J. S. Milsom (London, UK: Geological Society of London Memoir), 120–130.

Gasparon, M., and Varne, R. (1998). Crustal assimilation versus subducted sediment input in west Sunda arc volcanics: an evaluation. *Mineral. Petrol.* 64, 89–117.

Genrich, J. F., Bock, Y., McCaffrey, R., Prawirodirdjo, L., Stevens, C. W., Puntodewo, S. S. O., et al. (2000). Distribution of slip at the northern Sumatran fault system. *J. Geophys. Res.* 105, 28327–28341. doi: 10.1029/2000JB900158

Ghosal, D., Singh, S. C., Chauhan, A. P. S., and Hananto, N. D. (2012). New insights on the offshore extension of the Great Sumatran fault, NW Sumatra, from marine geophysical studies. *Geochem. Geophys. Geosys.* 13:Q0AF06. doi: 10.1029/2012GC004122

Gudmundsson, A. (1995). Infrastructure and mechanics of volcanic systems in Iceland. *J. Volcanol. Geother. Res.* 64, 1–22.

Hall, R., and Spakman, W. (2015). Mantle structure and tectonic history of SE Asia. *Tectonophysics* 658, 14–45. doi: 10.1016/j.tecto.2015.07.003

Harjono, H., Diament, M., Dubois, J., and Larue, M. (1991). Seismicity of the Sunda strait: evidence for crustal extension and volcanolgical implications. *Tectonics* 10, 17–30.

Heuret, A., and Lallemand, S. (2005). Plate motions slab dynamics and back-arc deformation. *Phys. Earth Planet. Inter.* 149, 31–51. doi: 10.1016/j.pepi.2004.08.022

Hickman, R. G., Dobson, P. F., van Gerven, M., Sagala, B. D., and Gunderson, R. P. (2004). Tectonic and stratigraphic evolution of the Sarulla graben geothermal area, North Sumatra, Indonesia. *J. Asian Earth Sci.* 23, 435–448. doi: 10.1016/S1367-9120(03)00155-X

Hollander, M., and Wolfe, D. A. (1973). *Non-Parametric Statistical Methods.* New York, NY: John Wiley.

Ito, T., Gunawan, E., Kimata, F., Tabei, T., Meilano I., Agustan, O. Y., et al. (2016). Co-seismic offsets due to two earthquakes ($M_w$ 6.1) along the Sumatran fault system derived from GNSS measurements. *Earth, Planets Space* 68:57. doi: 10.1186/s40623-016-0427-z

Jaxybulatov, K., Shapiro, N. M., Koulakov, I., Mordret, A., Landes, M., and Sens-Schönfelder, C. (2014). A large magmatic sill complex beneath the Toba caldera. *Science* 346, 617–619. doi: 10.1126/science.1258582

Kamesh Raju, K. A., Ray, D., Mudholkar, A., Murtya, G. P. S., Gahalaut, V. K., Samudrala, K., et al. (2012). Tectonic and volcanic implications of a cratered seamount off Nicobar Island, Andaman Sea. *J. Asian Earth Sci.* 56, 42–53. doi: 10.1016/j.jseaes.2012.04.018

Koulakov, I., Kasatkina, E., Shapiro, N. M., Jaupart, C., Vasilevsky, A., El Khrepy, S., et al. (2016). The feeder system of the Toba supervolcano from the slab to the shallow reservoir. *Nat. Communic.* 7:12228. doi: 10.1038/ncomms12228

Koulakov, I., Yudistira, T., Luehr, B. G., and Wandono (2009). P, S velocity and Vp/Vs ratio beneath the Toba caldera complex (northern Sumatra) from local earthquake tomography. *Geophys. J. Int.* 177, 1121–1139. doi: 10.1111/j.1365-246X.2009.04114.x

Kundu, B., Legrand, D., Gahalaut, K., Gahalaut, V. K., Mahesh, P., Kamesh Raju, K. A., et al. (2012). The 2005 volcano-tectonic earthquake swarm in the Andaman Sea: Triggered by the 2004 great Sumatra-Andaman earthquake. *Tectonics* 31:TC5009. doi: 10.1029/2012TC003138

Lallemand, S., Heuret, A., and Boutelier, D. (2005). On the relationships between slab dip, back-arc stress, upper plate absolute motion and crustal nature in subduction zones. *Geochem. Geophys. Geosyst.* 6:Q09006. doi: 10.1029/2005GC000917

Lallemant, H. G. A. (1996). Displacement partitioning and arc-parallel extension in the Aleutian volcanic island arc. *Tectonophysics* 256, 279–293.

Lara, L., Naranjo, J. A., and Moreno, H. (2004). Rhyodacitic fissure eruption in Southern Andes (Cordon Caulle; 40.5°S) after the 1960 (Mw:9.5) Chilean earthquake: a structural interpretation. *J. Volcanol. Geother. Res.* 138, 127–138. doi: 10.1016/j.jvolgeores.2004.06.009

Lassal, O., Huchon, P., and Harjono, H. (1989). Extension crustale dans le Detroit de la Sonde (Indonesie). Donnees de la sismique reflexion (champagne KRAKATAU). *C.R. Acad. Sci. Paris* 309, 205–212.

Lupi, M., and Miller, S. A. (2014). Short-lived tectonic switch mechanism for long-term pulses of volcanic activity after mega-thrust earthquakes. *Solid Earth* 5, 13–24. doi: 10.5194/se-5-13-2014

McCaffrey, R. (1992). Oblique plate convergence, slip vectors and forearc deformation. *J. Geophys. Res.* 97, 8905–8915.

McCaffrey, R., Zwick, P. C., Bock, Y., Prawirodirdjo, L., Genrich, J. F., Stevens, C. W., et al. (2000). Strain partitioning during oblique plate convergence in northern Sumatra: geodetic and seismologic constraints and numerical modelling. *J. Geophys. Res.* 105, 28363–28376. doi: 10.1029/1999JB900362

Mercier, J.-L., Carey-Gailhardis, E., and Sebrier, M. (1991). Paleostress determinations from fault kinematics: application to the Neotectonics of the Himalayas-Tibet and the Central Andes. *Phil. Trans. R. Soc. Lond.* 337, 41–52.

Moore, D. E., Hickman, S., Lockner, D. A., and Dobson, P. F. (2001). Hydrothermal minerals and microstructures in the Silangkitang geothermal field along the Great Sumatran fault zone, Sumatra, Indonesia. *GSA Bulletin* 113, 1179–1192. doi: 10.1130/0016-7606(2001)113<1179:HMAMIT>2.0.CO;2

Mount, V., and Suppe, J. (1992). Present-Day Stress Orientations Adjacent to Active Strike-Slip Faults: Califomia and Sumatra. *J. Geophys. Res.* 97, 11995–12013.

Muksin, U., Bauer, K., and Haberland, C. (2013). Seismic Vp and Vp/Vs structure of the geothermal area around Tarutung (North Sumatra, Indonesia) derived from local earthquake tomography. *J. Volcanol. Geother. Res.* 260, 27–42. doi: 10.1016/j.jvolgeores.2013.04.012

Muksin, U., Haberland, C., Nukman, M., Bauer, K., and Weber, M. (2014). Detailed fault structure of the Tarutung Pull-Apart Basin in Sumatra, Indonesia, derived from local earthquake data. *J. Asian Earth Sci.* 96, 123–131. doi: 10.1016/j.jseaes.2014.09.009

Nakano, M., Kumagai, H., Toda, S., Ando, R., Yamashina, T., Inoue, H., and Sunarjo (2010). Source model of an earthquake doublet that occurred in a pull-apart basin along the Sumatran fault, Indonesia. *Geophys. J. Int.* 181, 141–153. doi: 10.1111/j.1365-246X.2010.04511.x

Natawidjaja, D. H., Bradley, K., Daryono, M. R., Aribowo, S., and Herrin, J. (2017). Late Quaternary eruption of the Ranau Caldera and new geological slip rates of the Sumatran Fault Zone in Southern Sumatra, Indonesia. *Geosci. Lett* 4:21. doi: 10.1186/s40562-017-0087-2

Natawidjaja, D. H., and Triyoso, W. (2007). The Sumatran fault zone – from source to hazard. *J. Earthquake Tsunami* 1, 21–47.

Nobile, A., Pagli, C., Keir, D., Wright, T. J., Ayele, A., Ruch, J., et al. (2012). Dyke-fault interaction during the 2004 Dallol intrusion at the northern edge of the Erta Ale Ridge (Afar, Ethiopia). *Geophys. Res. Lett.* 39:L19305. doi: 10.1029/2012GL053152

Nukman, M., and Moeck, I. (2013). Structural controls on a geothermal system in the Tarutung Basin, north central Sumatra. *J. Asian Earth Sci.* 74, 86–96. doi: 10.1016/j.jseaes.2013.06.012

Ozawa, S., Nishimura, T., Suito, H., Kobayashi, T., Tobita, M., and Imakiire, T. (2011). Coseismic and postseismic slip of the 2011 magnitude-9 Tohoku-Oki earthquake. *Nature* 475, 373–377. doi: 10.1038/nature10227

Pallister, J. S., McCausland, W. A., Jonsson, S., Lu, Z., Zahran, H. M., El Hadidy, S., et al. (2010). Broad accommodation of rift-related extension recorder by dyke intrusion in Saudi Arabia. *Nat. Geosci.* 3, 708–712. doi: 10.1038/ngeo966

Pasquarè, F., and Tibaldi, A. (2003). Do transcurrent faults guide volcano growth? The case of NW Bicol Volcanic Arc, Luzon, Philippines. *Terra Nova* 15, 204–212. doi: 10.1046/j.1365-3121.2003.00484.x

Pesicek, J. D., Thurber, C. H., Widiyantoro, S., Engdahl, E. R., and DeShon, H. R. (2008). Complex slab subduction beneath northern Sumatra. *Geophys. Res. Lett.* 35:L20303. doi: 10.1029/2008GL035262

Pramumijoyo, S., and Sébrier, M. (1991). Neogene and Quaternary fault kinematics around the Sunda Strait area, Indonesia. *J. Southeast Asian Earth Sci.* 6, 137–145.

Prawirodirdjo, L., Bock, Y., and Genrich, J. F. (2000). One century of tectonic deformation along the Sumatran fault from triangulation and Global Positioning System surveys. *J. Geophs. Res.* 105, 28343–28361. doi: 10.1029/2000JB900150

Pritchard, M. E., Jay, J. A., Aron, F., Anderson, S. T., and Lara, L. E. (2013). Subsidence at southern Andes volcanoes induced by the 2010 Maule, Chile earthquake. *Nat. Geosci.* 6, 632–636. doi: 10.1038/ngeo1855

Reynard, B. (2016). Mantle hydration and Cl-rich fluids in the subduction forearc. *Progr. Earth Planet. Sci.* 3:9. doi: 10.1186/s40645-016-0090-9

Rock, N. M. S., Syah, H. H., Davis, A. E., Hutchison, D., Styles, M. T., and Lena, R. (1982). Permian to Recent Volcanism in Northern Sumatra, Indonesia: a Preliminary Study of its Distribution, Chemistry, and Peculiarities. *Bull. Volcanol.* 45, 127–152.

Rose, W. I., and Chesner, C. A. (1987). Dispersal of ash in the great Toba eruption, 75 ka. *Geology* 15, 913–917.

Rosenau, M., Melnick, D., and Echtler, H. (2006). Kinematic constraints on intra-arc shear and strain partitioning in the southern Andes between 38°S and 42°S latitude. *Tectonics* 25:4013. doi: 10.1029/2005TC001943

Rowland, J. V., Wilson, C. J. N., and Gravley, D. M. (2010). Spatial and temporal variations in magma-assisted rifting, Taupo Volcanic Zone, New Zealand. *J. Volcanol. Geother. Res.* 190, 89–108. doi: 10.1016/j.jvolgeores.2009.05.004

Rubin, A. M., and Pollard, D. D. (1988). Dike-induced faulting in rift zones of Iceland and Afar. *Geology* 16, 413–417.

Ruch, J., Vezzoli, L., De Rosa, R., Di Lorenzo, R., and Acocella, V. (2016). Magmatic control along a strike-slip volcanic arc: the central Aeolian arc (Italy). *Tectonics* 35, 407–424. doi: 10.1002/2015TC004060

Ruegg, J. C., Lepine, J. C., Tarantola, A., and Kasser, M. (1979). Geodetic measurements of rifting associated with a seismo-volcanic crisis in Afar. *Geophys. Res. Lett.* 6, 817–820.

Sakaguchi, K., Gilbert, H., and Zandt, G. (2006). Converted wave imaging of the Toba Caldera, Indonesia. *Geophys. Res. Lett.* 33:L20305. doi: 10.1029/2006GL027397

Sébrier, M., and Soler, P. (1991). "Tectonics and magmatism in the Peruvian Andes from late Oligocene time to the Present," in *Andean Magmatism and Its Tectonic Setting, Geological Society of America. Special Papers,* Vol. 265, eds Harmon and Rapela 259–278.

Sepulveda, F., Lahsen, A., Bonvalot, S., Cembrano, J., Alvarado, A., and Letelier, P. (2005). Morpho-structural evolution of the Còrdon Caulle geothermal region, Southern Volcanic Zone, Chile: insights from gravity and $^{40}Ar/^{39}Ar$ dating. *J. Volcanol. Geother. Res.* 148, 165–189. doi: 10.1016/j.jvolgeores.2005.03.020

Shabanian, E., Acocella, V., Gioncada, A., Ghasemi, H., and Bellier, O. (2012). Structural control on magmatism in intraplate collisional settings: extinct example from NE Iran and current analogues. *Tectonics* 31:TC3013. doi: 10.1029/2011TC003042

Shearer, P., and Burgmann, R. (2010). Lessons learned from the 2004 Sumatra-Andaman megathrust rupture. *Annu. Rev. Earth Planet. Sci.* 38, 103–131. doi: 10.1146/annurev-earth-040809-152537

Sieh, K., and Natawidjaja, D. (2000). Neotectonics of the Sumatran fault, Indonesia. *J. Geophys. Res.* 105, 28295–28326. doi: 10.1029/2000JB900120

Sigmundsson, F., Hooper, A., Hreinsdottir, S., Vogfjord, K. S., Ofeigsson, B. G., Heimisson, E. R., et al. (2015). Segmented lateral dyke growth in a rifting event at Bardarbunga volcanic system, Iceland. *Nature* 517, 151–158. doi: 10.1038/nature14111

Simons, M., Minson, S. E., Sladen, A., Ortega, F., Jiang, J., Owen, S. E., et al. (2011). The 2011 Magnitude 9.0 Tohoku-Oki Earthquake: mosaicking the megathrust from seconds to centuries. *Science* 332, 1421–1425. doi: 10.1126/science.1206731

Singer, B. S., Jicha, B. R., Harper, M. A., Naranjo, J. A., Lara, L. E., and Moreno-Roa, H. (2008). Eruptive history, geochronology and magmatic evolution of the Puyehue-Cordon Caulle volcanic complex, Chile. *GSA Bulletin* 120, 599–618. doi: 10.1130/B26276.1

Stankiewicz, J., Ryberg, T., Haberland, C., Fauzi, and Natawidjaja, D. (2010). Lake Toba volcano magma chamber imaged by ambient seismic noise tomography. *Geophys. Res. Lett.* 37:L17306. doi: 10.1029/2010GL044211

Subarya, C., Chlieh, M., Prawirodirdjo, L., Avouac, J. P., Bock, Y., Sieh, K., et al. (2006). Plate boundary deformation associated with the great Sumatra-Andaman earthquake. *Nature* 440, 46–51. doi: 10.1038/nature04522

Takada, Y., and Fukushima, Y. (2013). Volcanic subsidence triggered by the 2011 Tohoku earthquake in Japan. *Nat. Geosci.* 6, 637–641. doi: 10.1038/ngeo1857

Tibaldi, A. (1992). The role of transcurrent intra-arc tectonics in the configuration of a volcanic arc. *Terra Nova* 4, 567–577, doi: 10.1111/j.1365-3121.1992.tb00598.x.

Tibaldi, A., Pasquaré, F., and Tormey, D. (2010). "Volcanism in reverse and strike-slip fault settings," in *New Frontiers in Integrated Solid Earth Sciences*, eds S. Cloetingh and J. Negendank (New York, NY: Springer), 315–348.

Tobisch, O., and Cruden, A. R. (1995). Fracture controlled magma conduits in an obliquely convergent continental magmatic arc. *Geology* 23, 941–944.

Tryggvason, E. (1994). Surface deformation at the Krafla volcano, North Iceland, 1982-1992. *Bull. Volcanol.* 56, 98–107.

Vazquez, J. A., and Reid, M. R. (2004). Probing the accumulation history of the voluminous Toba magma. *Science* 305, 991–994. doi: 10.1126/science.1096994

Vigny, C., Socquet, A., Peyrat, S., Ruegg, J.-C., Métois, M., Madariaga, R., et al. (2011). The 2010 *Mw* 8.8 Maule Megathrust Earthquake of Central Chile, Monitored by GPS. *Science* 332, 1417–1421. doi: 10.1126/science.1204132

Walter, T. R., and Amelung, F. (2007). Volcanic eruptions following M≥9 megathrust earthquakes: implications for the Sumatra-Andaman volcanoes. *Geology* 35, 539–542. doi: 10.1130/G23429A.1

Wang, K., Hu, Y., Bevis, M., Kendrick, E., Smalley, R., Vargas, R. B., et al. (2007). Crustal motion in the zone of the 1960 Chile earthquake: detangling earthquake-cycle deformation and forearc-sliver Translation. *Geochem. Geophys. Geosys.* 8:Q10010. doi: 10.1029/2007GC001721

Weller, O., Lange, D., Tilmann, F., Natawidjaja, D., Rietbrock, A., Collings, R., et al. (2012). The structure of the Sumatran Fault revealed by local seismicity. *Geophys. Res. Lett.* 39:L01306. doi: 10.1029/2011GL050440

Widiwijayanti, C., Deverchere, J., Louat, R., Sebrier, M., Harjono, H., Diament, M., et al. (1996). Aftershock sequence of the 1994, Mw 6.8, Liwa earthquake (Indonesia): seismic rupture process in a volcanic arc. *Geophys. Res. Lett.* 23, 3051–3054.

Wright, T. J., Ebinger, C., Biggs, J., Ayele, A., Yirgu, G., Keir, D., et al. (2006). Magma maintained rift segmentation at continental rupture in the 2005 Afar dyking episode. *Nature* 442, 291–294. doi: 10.1038/nature04978

Xu, W., Ruch, J., and Jónsson, S. (2015). Birth of two volcanic islands in the southern Red Sea. *Nature Communications* 6:7104. doi: 10.1038/ncomms8104

**Conflict of Interest Statement:** The authors declare that the research was conducted in the absence of any commercial or financial relationships that could be construed as a potential conflict of interest.